Amplifying Genetic Logic Gates

Jerome Bonnet *et al.*

Science **340**, 599 (2013);
DOI: 10.1126/science.1232758

Science (print ISSN 0036-8075; online ISSN 1095-9203) is published weekly, except the last week in December, by the American Association for the Advancement of Science, 1200 New York Avenue NW, Washington, DC 20005.

chains that could be derivatized, it should be possible to tune their properties for applications such as vehicles for drug and biomolecule delivery, cages for trapping functional enzyme cascades that allow flux of starting materials and products, components of sensing systems, and new frameworks for the development of protocells (*24*).

References and Notes

1. H. F. Lodish, *Molecular Cell Biology* (W.H. Freeman, New York, ed. 6, 2008).
2. S. Tanaka *et al*., *Science* **319**, 1083 (2008).
3. C. M. Agapakis, P. M. Boyle, P. A. Silver, *Nat. Chem. Biol.* **8**, 527 (2012).
4. D. A. Hammer, N. P. Kamat, *FEBS Lett.* **586**, 2882 (2012).
5. M. Uchida *et al*., *Adv. Mater.* **19**, 1025 (2007).
6. R. M. Capito, H. S. Azevedo, Y. S. Velichko, A. Mata, S. I. Stupp, *Science* **319**, 1812 (2008).
7. F. Boato *et al*., *Angew. Chem. Int. Ed. Engl.* **46**, 9015 (2007).
8. S. Raman, G. Machaidze, A. Lustig, U. Aebi, P. Burkhard, *Nanomedicine* **2**, 95 (2006).
9. N. P. King *et al*., *Science* **336**, 1171 (2012).
10. Y. T. Lai, D. Cascio, T. O. Yeates, *Science* **336**, 1129 (2012).
11. B. Wörsdörfer, K. J. Woycechowsky, D. Hilvert, *Science* **331**, 589 (2011).
12. J. C. Sinclair, K. M. Davies, C. Vénien-Bryan, M. E. M. Noble, *Nat. Nanotechnol.* **6**, 558 (2011).
13. J. D. Brodin *et al*., *Nat. Chem.* **4**, 375 (2012).
14. M. M. Pires, J. Lee, D. Ernenwein, J. Chmielewski, *Langmuir* **28**, 1993 (2012).
15. E. H. C. Bromley, K. Channon, E. Moutevelis, D. N. Woolfson, *ACS Chem. Biol.* **3**, 38 (2008).
16. A. N. Lupas, M. Gruber, *Adv. Protein Chem.* **70**, 37 (2005).
17. D. N. Woolfson, *Adv. Protein Chem.* **70**, 79 (2005).
18. J. M. Fletcher *et al*., *ACS Synth. Biol.* **1**, 240 (2012).
19. E. H. C. Bromley, R. B. Sessions, A. R. Thomson, D. N. Woolfson, *J. Am. Chem. Soc.* **131**, 928 (2009).
20. Materials and methods are available as supplementary materials on *Science* Online.
21. R. L. Harniman *et al*., *Nanotechnology* **23**, 085703 (2012).
22. www.quorumtech.com/pdf/SputterCoatingTechniques/Sputter_coating_technical_brief.pdf
23. G. Offer, R. Sessions, *J. Mol. Biol.* **249**, 967 (1995).
24. S. S. Mansy *et al*., *Nature* **454**, 122 (2008).
25. E. K. O'Shea, R. Rutkowski, P. S. Kim, *Science* **243**, 538 (1989).

Acknowledgments: We thank the Woolfson group for valuable discussions; the BBSRC for funding to D.N.W. and P.J.B. (BB/G008833/1) and for a studentship to A.L.B.; and the EPSRC for studentships to R.L.H. and T.H.S. J.M. is supported by a Wellcome University Award. We are grateful to the University of Bristol Advanced Computing Research Centre and the eInfraStructureSouth Consortium for high-performance computing; and Jonathan Jones and the EM Unit (EMU) School of Chemistry University of Bristol for EM access. The peptides described have been added to the Pcomp database for synthetic biology (http://coiledcoils.chm.bris.ac.uk/pcomp/index.php).

Supplementary Materials

www.sciencemag.org/cgi/content/full/science.1233936/DC1
Materials and Methods
Figs. S1 to S15
Tables S1 to S3
References (*26*–*38*)
Movie S1

11 December 2012; accepted 11 March 2013
Published online 11 April 2013;
10.1126/science.1233936

Amplifying Genetic Logic Gates

Jerome Bonnet, Peter Yin,* Monica E. Ortiz, Pakpoom Subsoontorn, Drew Endy†

Organisms must process information encoded via developmental and environmental signals to survive and reproduce. Researchers have also engineered synthetic genetic logic to realize simpler, independent control of biological processes. We developed a three-terminal device architecture, termed the transcriptor, that uses bacteriophage serine integrases to control the flow of RNA polymerase along DNA. Integrase-mediated inversion or deletion of DNA encoding transcription terminators or a promoter modulates transcription rates. We realized permanent amplifying AND, NAND, OR, XOR, NOR, and XNOR gates actuated across common control signal ranges and sequential logic supporting autonomous cell-cell communication of DNA encoding distinct logic-gate states. The single-layer digital logic architecture developed here enables engineering of amplifying logic gates to control transcription rates within and across diverse organisms.

Researchers have used genetically encoded logic, data storage, and cell-cell communication to study and reprogram living systems, explore biomolecular computing, and improve cellular therapeutics (*1*–*9*). Most approaches to engineering cell-based logic champion two-terminal device architectures upon which gate-gate layering, similar to conventional electronics, is used to realize all logic functions (*10*, *11*). Despite recent advances (*11*, *12*), such designs are difficult to scale because of problems associated with reusing regulatory molecules within the self-mixing environments of individual cells. As representative examples, a single-cell two-input "exclusive or" (XOR) gate, a function whose output is high only if the inputs are different, required controlled expression of four gate-specific regulatory molecules from four plasmids (*12*); an amplifying "exclusive nor" (XNOR) gate, high output only if inputs are equal, has not been demonstrated within single cells (*10*).

Department of Bioengineering, Y2E2-269B, 473 Via Ortega, Stanford, CA 94305–4201, USA.

*Present address: Department of Biology, University of Pennsylvania, Philadelphia, PA 19104, USA.
†Corresponding author. E-mail: endy@stanford.edu

We instead sought a device architecture in which the same regulatory molecules could be simply reused to implement all logic gates within a single logic layer (*13*). We also sought to decouple the signals controlling gate switching from gate inputs and outputs. Realizing both goals would enable straightforward engineering of distinct gates with constant switching thresholds and support signal gain and amplification if desired. Lastly, we wanted all gate signals to be encoded via a common signal carrier supporting connectivity within natural systems and across a diverse family of engineered genetic devices (*14*).

We combined earlier concepts (*14*–*17*) to invent a transistor-like three terminal device (*18*) termed the transcriptor. Independent control signals govern transcriptor logic elements that regulate transcriptional "current," defined by the flow of RNA polymerase along DNA (Fig. 1A). Gate input and output signals are transcription rates at positions on DNA marking logic element boundaries. Logic elements use asymmetric transcription terminators as reversible check valves that disrupt RNA polymerase flow in only one of two possible orientations (Fig. 1B). Recombinases catalyze unidirectional inversion of DNA within opposing recognition sites (Fig. 1B) or deletion of DNA between aligned sites (Fig. 1C), providing independent control over the orientation or presence of one or more terminators. Stated differently, we developed a device architecture similar to a transistor but leveraged unique properties of genetic regulation to implement all gates without requiring that multiple instances of simpler gates be connected in series (i.e., without layering) (*18*, *19*).

For example, a transcriptor XOR logic element requires bracketing one asymmetric transcription terminator with two pairs of opposing recombination sites recognized by independent integrases (Fig. 1D). If neither integrase is expressed, then the terminator blocks transcription (Fig. 1D, top). Expression of either integrase alone inverts the DNA encoding the terminator and allows transcription to flow through the transcriptor (Fig. 1D, middle). Expression of both integrases inverts and then restores the original orientation of the terminator, again blocking transcription (Fig. 1D, bottom). A complete XOR gate requires placing an XOR logic element within a three-terminal device in which integrase expression is controlled by two independent control signals (Fig. 1E).

We designed additional transcriptor logic elements encoding Boolean OR, NOR, XNOR, and AND functions for use within a common gate architecture (Fig. 2 and fig. S1). Straightforward changes only to logic element DNA were sufficient to design functionally distinct gates expected to be responsive to identical control signals. Designing a transcriptor-only "not and" (NAND) element, low output only if both control signals are high, proved more challenging. We instead used a hybrid architecture that combines flipping of a terminator along with a constitutive promoter. Although noncanonical, the NAND gate still responds to the same control signals while exhibiting varied output levels (below).

Transcriptor elements allowing unidirectional processing of DNA produce permanent gates that implement write-once logic operations. However, recombination directionality factors (RDFs) can reverse DNA inversion by integrases (*20*). We designed rewritable transcriptor elements in which controlled expression of RDFs, given constitutive integrase expression, should implement reversible logic and demonstrated a reversible buffer gate controlled by a single RDF (figs. S2 and S3); reversible gates require the same number of regulated factors as permanent gates (e.g., two RDFs versus two integrases). Permanent gates are useful for applications requiring tracking or processing of historical signals (e.g., terminal differentiation during development or accumulated responses to asynchronous environmental cues), whereas reversible gates support multicycle computing (e.g., a synchronized cell division cycle counter).

We selected unidirectional serine integrases from bacteriophages TP901-1 and Bxb1 to control gate switching; these recombinases do not require host cofactors and have been shown to function in bacteria, fungi, plants, and animals (*21*). We recently implemented a rewritable digital latch by using the Bxb1 integrase and RDF to repeatedly flip a DNA memory element between two states (*5*); this class of latches are controlled by continuous transcription signals (i.e., analog inputs) that produce recombinase proteins sufficient to flip (or not) a DNA element (i.e., digital output) and thus can be abstracted and reused (*22*) as analog-to-digital converters.

We made a recombination control plasmid expressing the TP901-1 and Bxb1 integrases under the control of exogenous arabinose (ara) and anhydrotetracycline (aTc) induction, respectively (*23*). We measured the propensities of TP901-1 and Bxb1 integrases to recognize and process specific DNA recombination sites (fig. S4A). We fitted abstracted Hill functions representing observed DNA processing propensities given increasing expression levels for each integrase alone (fig. S4B). We defined logic function models specific to each gate (fig. S4C) and predicted the expected behavior of multi-input gates directly from single-integrase Hill functions (Fig. 2).

We constructed low-copy plasmids encoding AND, OR, XOR, NAND, NOR, and XNOR logic elements between a standard strong prokaryotic promoter (input signal source) and green fluorescent protein (GFP) expression cassette (indirect output signal reporter) (*23*). We measured bulk GFP levels from bacterial cultures expressing varying amounts of TP901-1 and Bxb1 integrases controlling the six Boolean gates. Observed GFP expression patterns were well matched to predictions for all gates (Fig. 2); exact output levels varied among and within some gates (described below).

Transcriptor-based gates use discrete enzymatic processing of DNA to modulate RNA polymerase flow through logic elements. We thus expected that single cells might exhibit discontinuous (e.g., all or none) responses to small changes in control signals. For example, we measured fluorescence output distributions among single cells exposed to low or high control signals and found a single threshold defining distinct low/high outputs across all gates (Fig. 2, red vertical line). To better study control signal digitization (i.e., the extent to which gate outputs are more digital than gate control signals across small changes in control signals), we compared changes in gate outputs to increasing control signals by using a common reporter (figs. S5 to S8). For example, we found that XOR gates switch completely between 0.2 and 2 ng/ml aTc and 0.0001 to 0.001% ara, whereas both control signals increase gradually across these inducer ranges (Fig. 3, A and B, and figs. S6 to S8). We defined a digitization error rate as the combined probability of scoring false high or low gate outputs in response to intermediate control signal changes, optimized thresholds for controllers and gates that best discriminate between putative low and high outputs, and quantified digitization error rates for each gate. AND, OR, XOR, and XNOR gates digitized aTc-induced control signals to varying degrees, whereas AND, OR, NOR, XOR, and XNOR gates digitized ara-induced signals (Fig. 3, C and D); no gates reduced digitization (Fig. 3, C and D), and all gates realized digital outputs in response to low/high control signals (Fig. 2).

Changes in gate outputs must be compared directly to changes in gate control signals to determine whether gates function as amplifiers (*24*, *25*). We calculated population-average GFP levels for each control signal and gate outputs (fig. S5). We directly compared changes in gate outputs to the changes in gate control signals needed to activate gate switching, both for absolute (figs. S9 and S10) and normalized (Fig. 4) expression levels. We evaluated all gates across control-signal ranges needed to drive the least-

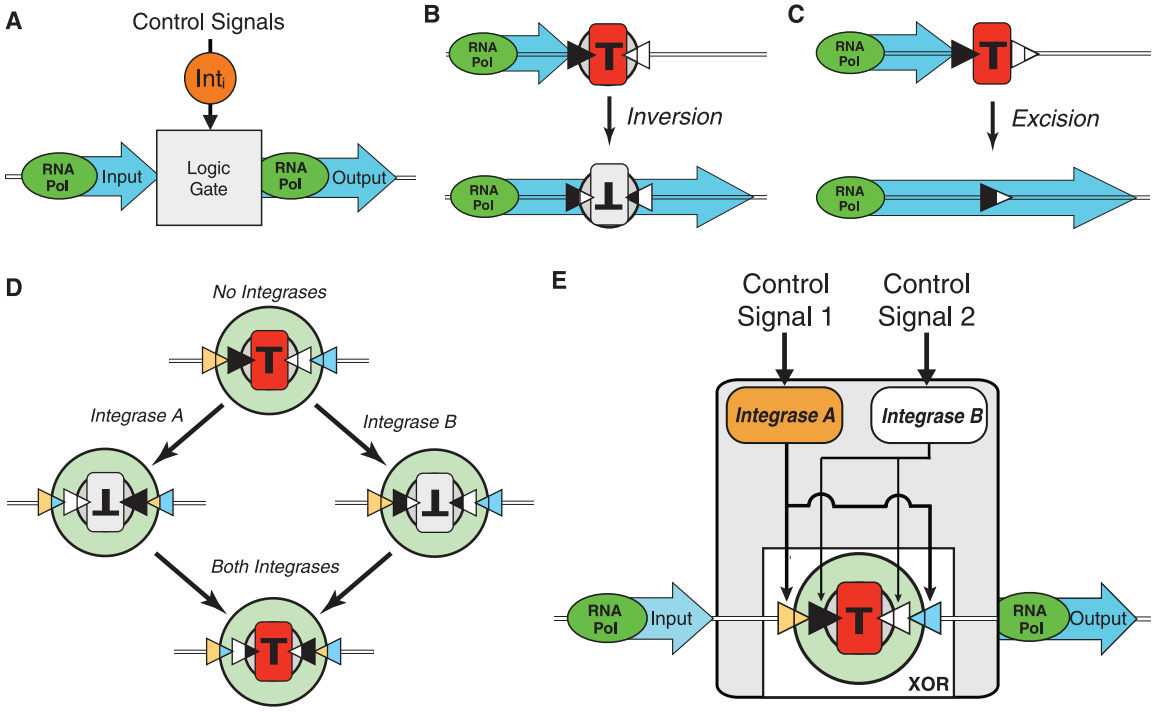

Fig. 1. Using transcriptors to implement three-terminal Boolean integrase logic gates. (**A**) Three-terminal transcriptor-based gates use integrase (Int) control signals to modulate RNA polymerase (RNA Pol) flow between a separate gate input and output. (**B**) A canonical transcriptor element wherein an asymmetric transcription terminator (T) blocks transcriptional current in one orientation (red) or, when flipped, the opposite orientation (gray). Opposing recombination sites (black/white triangles) flank the terminator and direct flipping by an integrase. (**C**) Integrases can also excise DNA between aligned recombination sites. (**D**) State diagram for a transcriptor "exclusive or" (XOR) logic element: Opposing sites recognized by two independent integrases (blue/orange and black/white) are nested and flank one terminator. Recombination can produce four distinct states controlling terminator orientation. (**E**) The logic element from (D) within a three-terminal Boolean integrase XOR gate such that gate output is high only if control signals are different.

responsive gate (NAND) and did not normalize outputs via subtraction of lowest values, which otherwise greatly increases fold-change estimates. All gates generate increased absolute and fold-change differences in expressed output protein levels relative to those produced from the integrase controllers (Fig. 4 and figs. S9 and S10).

We confirmed that permanent transcriptor-based gates support sequential logic based on the heritable storage of logic element states in response to asynchronous control signals. For example, cells encoding AND and XNOR gates were exposed to various patterns of integrase control signals, recording and generating appropriate outputs across ~40 cell doublings (fig. S11). Building from these results, we engineered cell-cell communication of DNA (*7*) encoding logic gates at different stages of gate activation (fig. S12), a feature unique to gates whose operation involves direct processing of DNA. We also assayed recombination response times, finding that 15-min control-signal pulses were sufficient to activate integrase-mediated switching (fig. S13 and movie S1).

During the course of responding to reviewer questions and preparing the final version of this manuscript, a system of two terminal logic gates was described by Siuti *et al*. based on flipping terminator, promoter, and gene elements (*26*). The family of Boolean integrase logic gates introduced here differs in the consistent use of a three-terminal device architecture that decouples logic-gate operation from both input and output signals, enabling simple tuning via changes to the transcription input signal (fig. S14) and ready reuse (e.g., reprogramming of natural transcription

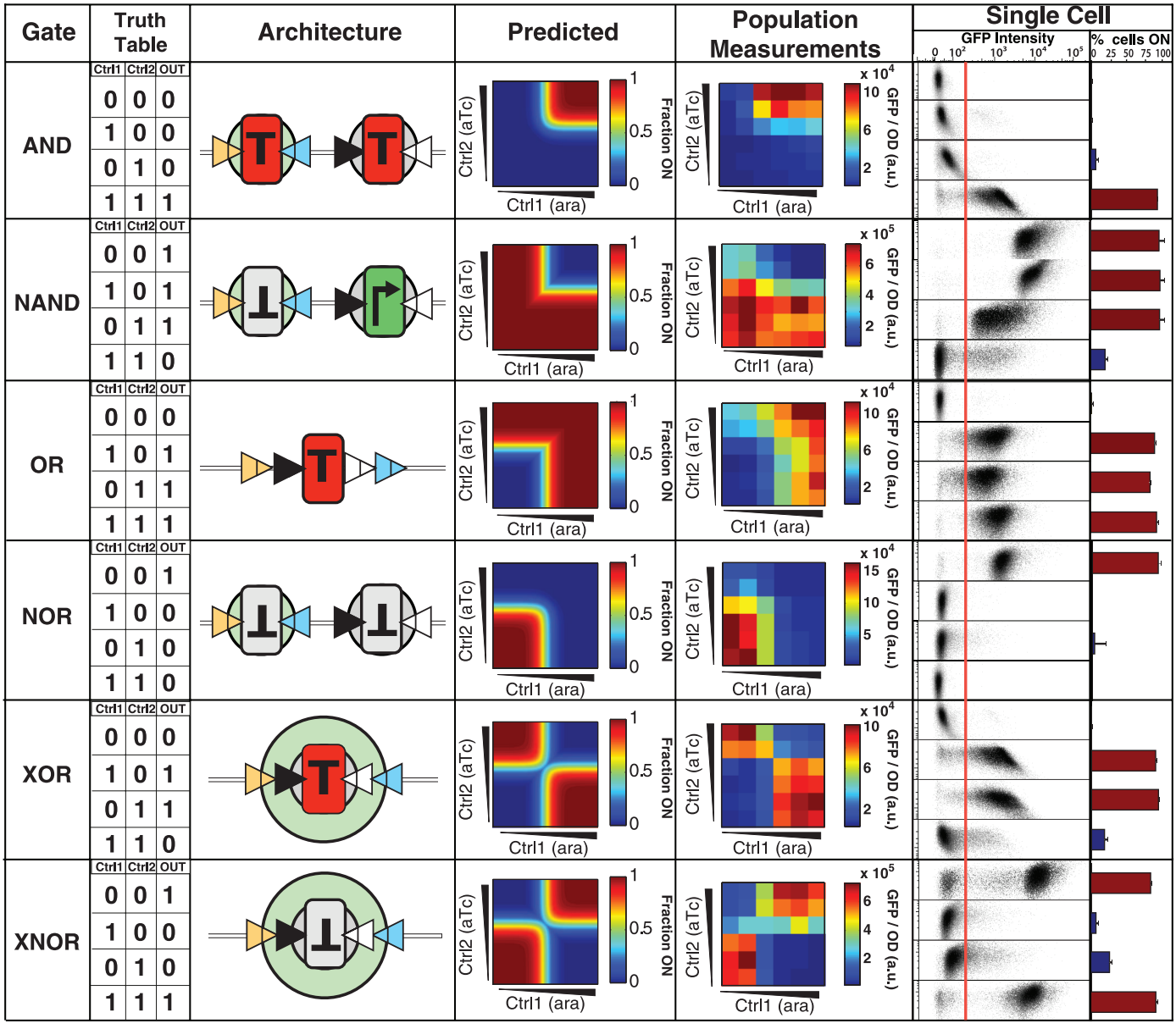

Fig. 2. Predicted and observed logic-gate performance plus digital-output thresholding. (Gate) Boolean logic functions. (Truth Table) Logical relationships between control (Ctrl) signals and output. (Architecture) Transcriptor element configurations for use in permanent Boolean integrase logic gates, including a constitutive promoter (NAND, green rightward arrow). (Predicted) Expected fraction of cells containing gates in a high-output state (heat map) calculated as described (*23*). (Population Measurements) Gate outputs assayed via plate reader for bulk cultures (*23*). Inducer concentrations are 0, 0.02, 0.2, 2, 20, and 200 ng/ml for aTc and 0, 0.0001, 0.001, 0.01, 0.1, and 1% weight/volume (w/v) for ara. (Single Cell, GFP Intensity) Distribution of gate outputs [*x* axis GFP output measured in arbitrary units (a.u.); *y* axis side scatter] among single cells responding to control signals, as per gate-specific truth tables. A common output threshold segregates low/high outputs across all gates (vertical red line). Inducer concentrations are 200 ng/ml for aTc and 1% w/v for ara. (% Cells On) Fraction of cells encoding high outputs when scored by using a common output threshold.

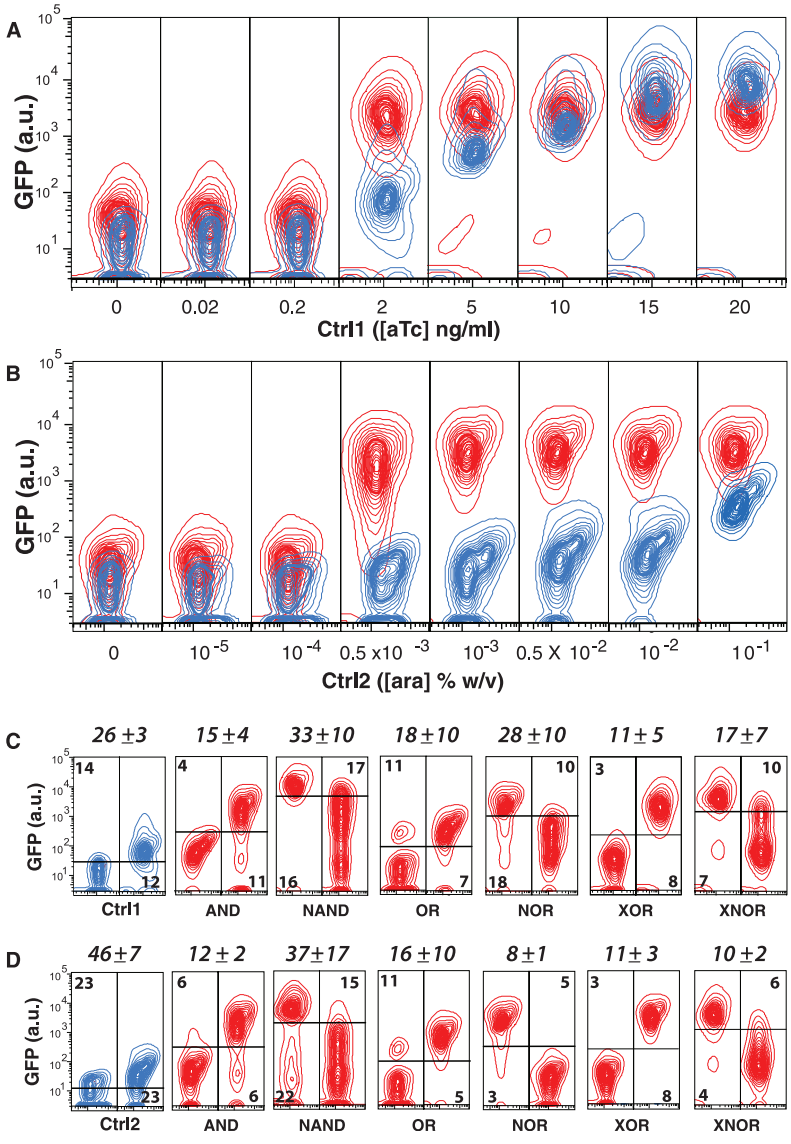

Fig. 3. Digitization of control signals. (**A**) Distribution of XOR outputs among single cells (red contours) responding to an increasing control signal (blue contours). Each contour interval encompasses 5% of all cells; thick contours surround 50% of the total population. *y* axis, GFP output measured in arbitrary units (a.u.); *x* axis, side scatter at noted inducer concentrations. (**B**) As in (A) but for the second control signal. (**C**) Gate switching and digitization errors across an intermediate control signal change (0.2 to 2 ng/ml aTc, left/right of each frame). Gate-specific digitization thresholds (horizontal bars) were optimized and used to quantify fractions of false high cells given a low control signal and vice versa. Numbers within frames are high-given-low and low-given-high error rates. Numbers above boxes are combined error rates with standard deviation from three independent experiments. (**D**) As in (C), but in response to an intermediate change in the second control signal (1×10^{-4} to 0.5×10^{-2} ara, left/right of each frame).

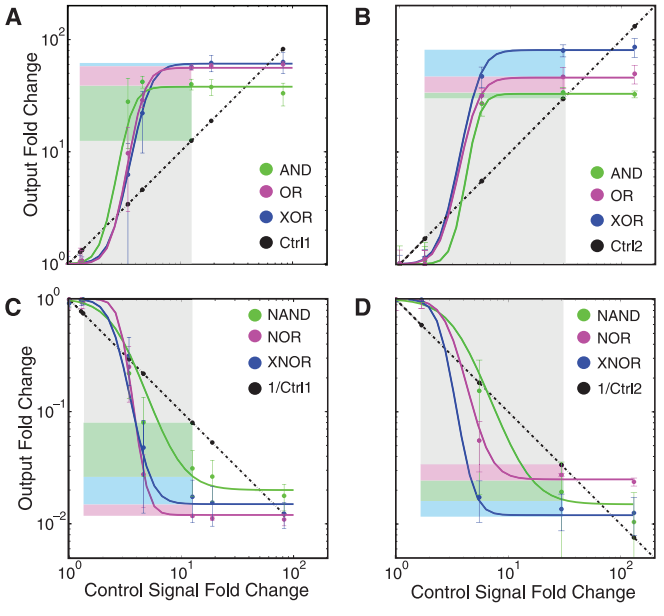

Fig. 4. Gain and amplification across common control signal ranges. Population-average response of amplifier gates to (**A**) increasing ara-mediated expression of TP901-1 integrase and (**B**) increasing aTc-mediated expression of Bxb1 integrase. Changes in output GFP levels produced by gates (colored lines) are directly compared to changes in control signals required for gate switching (increasing straight dashed lines). The response of each control signal to itself (gray boxes) is shown to highlight gate-specific amplification of control signals (colored boxes). (**C** and **D**) Responses of inverting amplifier gates. As in (A) and (B), except that fold changes for control signals are inverted (decreasing straight dashed lines) (figs. S8 and S10). Error bars indicate SD across three independent experiments.

systems by seamless integration of transcriptor logic elements within natural operons). Also, by separating gate inputs from gate control signals and by using a strong input signal modulated by an efficient asymmetric terminator, we were able to demonstrate and quantify signal amplification for all gates (Figs. 3 and 4).

Output signal levels vary within and among the gates reported here (Figs. 2 and 3 and figs. S9 and S10), although not more so than existing genetic logic. We believe that most variation arises from differences in RNA secondary structures well known to influence mRNA stability and translation initiation rates (fig. S15); such variation might be eliminated by using recently reported mRNA processing methods (*24*, *27*). Further work is also required to realize precise level matching across all gates, and directed evolution of increasingly asymmetric terminators may be needed to reduce low output levels for most gates (fig. S10); additional gate-specific tuning of NAND would be required given its noncanonical logic element. Nevertheless, existing gates already support single-layer programmable digital logic, control-signal amplification, sequential logic, and cell-cell communication of intermediate logic states. Multi-input gates supporting high "fan-in" could be realized by using additional integrases (*28*) (fig. S16). Transcriptor-based gates can also likely be directly combined with other logic families to expand the power of engineered genetic computers. All logic gates and uses thereof demonstrated or disclosed here have been contributed to the public domain via the BioBrick Public Agreement (*29*).

References and Notes

1. B. Wang, M. Buck, *Trends Microbiol.* **20**, 376 (2012).
2. Y. Benenson, *Nat. Rev. Genet.* **13**, 455 (2012).
3. T. Miyamoto, S. Razavi, R. DeRose, T. Inoue, *ACS Synth. Biol.* **2**, 72 (2013).
4. D. R. Burrill, P. A. Silver, *Cell* **140**, 13 (2010).
5. J. Bonnet, P. Subsoontorn, D. Endy, *Proc. Natl. Acad. Sci. U.S.A.* **109**, 8884 (2012).
6. S. Basu, Y. Gerchman, C. H. Collins, F. H. Arnold, R. Weiss, *Nature* **434**, 1130 (2005).
7. M. E. Ortiz, D. Endy, *J. Biol. Eng.* **6**, 16 (2012).
8. Y. Y. Chen, M. C. Jensen, C. D. Smolke, *Proc. Natl. Acad. Sci. U.S.A.* **107**, 8531 (2010).
9. Z. Xie, L. Wroblewska, L. Prochazka, R. Weiss, Y. Benenson, *Science* **333**, 1307 (2011).
10. A. Tamsir, J. J. Tabor, C. A. Voigt, *Nature* **469**, 212 (2011).
11. T. S. Moon, C. Lou, A. Tamsir, B. C. Stanton, C. A. Voigt, *Nature* **491**, 249 (2012).
12. S. Ausländer, D. Ausländer, M. Müller, M. Wieland, M. Fussenegger, *Nature* **487**, 123 (2012).
13. For example, converting a NOR gate repressed by transcription factors to an OR gate activated by transcription factors requires changing how proteins interact with RNA polymerase (from competitive binding and occlusion to recruitment and initiation) and simultaneous reworking of the basal activity for core promoter elements (from a constitutively active promoter that can be repressed to a weak promoter that does not spontaneously initiate transcription yet that transcription factors activate).
14. C. Wadey, I. Deese, D. Endy, "Common signal carriers," in *Adventures in Synthetic Biology* (OpenWetWare and Nature Publishing Group New York, 2005), chap. 3; available online at http://hdl.handle.net/1721.1/46337.
15. T. S. Ham, S. K. Lee, J. D. Keasling, A. P. Arkin, *PLoS ONE* **3**, e2815 (2008).
16. A. E. Friedland *et al.*, *Science* **324**, 1199 (2009).
17. P. A. Varadarajan, D. Del Vecchio, *IEEE Trans. Nanobioscience* **8**, 281 (2009).
18. J. Bardeen, W. Brattain, *Phys. Rev.* **74**, 230 (1948).
19. With transistor-based logic, gates use a base, emitter, and collector architecture that classically only allows for control of electrical current at one point on a wire by a single signal. Transcriptor-based logic allows RNA polymerase flow at a single point on DNA to be controlled, in theory, by as many independent recombinases as needed.
20. J. A. Lewis, G. F. Hatfull, *Nucleic Acids Res.* **29**, 2205 (2001).
21. W. R. A. Brown, N. C. O. Lee, Z. Xu, M. C. M. Smith, *Methods* **53**, 372 (2011).
22. B. Canton, A. Labno, D. Endy, *Nat. Biotechnol.* **26**, 787 (2008).
23. Materials and methods are available as supplementary materials on *Science* Online.
24. C. Lou, B. Stanton, Y.-J. Chen, B. Munsky, C. A. Voigt, *Nat. Biotechnol.* **30**, 1137 (2012).
25. L. Pasotti, N. Politi, S. Zucca, M. G. Cusella De Angelis, P. Magni, *PLoS ONE* **7**, e39407 (2012).
26. P. Siuti, J. Yazbek, T. K. Lu, *Nat. Biotechnol.* (2013).
27. L. Qi, R. E. Haurwitz, W. Shao, J. A. Doudna, A. P. Arkin, *Nat. Biotechnol.* **30**, 1002 (2012).
28. G. F. Hatfull *et al.*, *J. Virol.* **86**, 2382 (2012).
29. https://biobricks.org/bpa/

Acknowledgments: We thank M. Juul, T. Knight, S. Kushner, C. Smolke, B. Townshend, the Endy and Smolke labs, and the Stanford Shared FACS Facility. Funding was provided by the NSF Synthetic Biology Engineering Research Center, Stanford Center for Longevity, Stanford Bio-X, the Townshend/Lamarre Family Foundation, and the Siebel Foundation. DNA sequences are available in GenBank (accession nos. KC529324 to KC529332). DNA constructs will be made available via Addgene.

Supplementary Materials

www.sciencemag.org/cgi/content/full/science.1232758/DC1
Materials and Methods
Figs. S1 to S15
Appendices S1 to S4
References (*30*–*44*)
Movie S1

14 November 2012; accepted 13 March 2013
Published online 28 March 2013;
10.1126/science.1232758

Controlled Flight of a Biologically Inspired, Insect-Scale Robot

Kevin Y. Ma,*† Pakpong Chirarattananon,† Sawyer B. Fuller, Robert J. Wood

Flies are among the most agile flying creatures on Earth. To mimic this aerial prowess in a similarly sized robot requires tiny, high-efficiency mechanical components that pose miniaturization challenges governed by force-scaling laws, suggesting unconventional solutions for propulsion, actuation, and manufacturing. To this end, we developed high-power-density piezoelectric flight muscles and a manufacturing methodology capable of rapidly prototyping articulated, flexure-based sub-millimeter mechanisms. We built an 80-milligram, insect-scale, flapping-wing robot modeled loosely on the morphology of flies. Using a modular approach to flight control that relies on limited information about the robot's dynamics, we demonstrated tethered but unconstrained stable hovering and basic controlled flight maneuvers. The result validates a sufficient suite of innovations for achieving artificial, insect-like flight.

Using flapping wings and tiny nervous systems, flying insects are able to perform sophisticated aerodynamic feats such as deftly avoiding a striking hand or landing on flowers buffeted by wind. How they perform these feats—from sensorimotor transduction to the unsteady aerodynamics of their wing motions—is just beginning to be understood (*1*–*3*), aided in part by simulation (*4*) and scaled models (*5*). Motivated by a desire for tiny flying robots with comparable maneuverability, we seek to create a robotic vehicle that mirrors these basic flight mechanics of flies. At the scale of flies, no such vehicle has been demonstrated to date because of the severe miniaturization challenges that must be overcome for an insect-sized device (*6*). Conventional technologies for macroscale aircraft propulsion and manufacturing are not viable for millimeter-scale robots because of inefficiencies that arise from force scaling, suggesting a biologically inspired solution based on flapping wings (*7*–*9*). Here, we report an aggregation of innovations in design, manufacturing, actuation, and control to create an insect-scale flying robot—a robotic fly—that successfully demonstrates tethered but unconstrained flight behavior reminiscent of flying insects.

For inspiration of form and function, we used *Diptera* (flies) as a model system because of the relative simplicity of the flight apparatus—flies by classification have only two wings—and the exemplary aerial agility that they exhibit. Dipteran flight has been well-studied (*5*, *10*–*18*), and it is understood that insect wings undergo a complex trajectory defined by three rotational degrees of freedom (*10*). This has been simplified in the robotic fly to a reciprocating flapping motion in which the wings' pitch rotation is regulated with passive compliant flexures (*19*)—an enabling simplification for mechanism design and manufacture. Key aspects of the oscillatory wing motion are the flapping frequency and wing stroke amplitude; the robotic fly achieves 120 Hz and 110°, respectively, similar to the 130-Hz wing beat

School of Engineering and Applied Sciences and the Wyss Institute for Biologically Inspired Engineering, Harvard University, Cambridge, MA 02138, USA.

*Corresponding author. E-mail: kevinma@seas.harvard.edu
†These authors contributed equally to this work.

Supplementary Materials for

Amplifying Genetic Logic Gates

Jerome Bonnet, Peter Yin, Monica E. Ortiz, Pakpoom Subsoontorn, Drew Endy*

*To whom correspondence should be addressed. E-mail: endy@stanford.edu

Published 28 March 2013 on *Science* Express
DOI: 10.1126/science.1232758

This PDF file includes:

Other Supplementary Material for this manuscript includes the following:
available at www.sciencemag.org/cgi/content/full/science.1232758/DC1

Materials and Methods

1. Molecular biology

Coding sequences for Bxb1 and TP901 integrases were synthesized by DNA 2.0 (Menlo Park, CA, USA). Logic elements were synthesized by IDT (Carlsbad, USA). Plasmids and parts encoding pBAD/AraC ((*30*), iGEM registry accession number: BBa_I0500), superfolder GFP ((*31*), iGEM registry accession number: BBa_I746916) and pTetO promoter ((*32)*, iGEM registry accession number: Bba_R0040), and terminators B0015 (iGEM registry accession number: B0015) and J61048 (iGEM registry accession number:J61048) were obtained from the iGEM Registry of Standard Biological Parts (http://partsregistry.org).

We chose terminator B0015 as it has already been measured as (i) having a strong forward termination efficiency (T.E. ~98%) and (ii) having asymmetric termination efficiencies between its forward and its reverse orientations (reported reverse T.E. between ~30% and ~60%). No reverse efficiency information was available for J61048 but it was measured as having a strong forward T.E. (~98%) and our experiments show that it is an asymmetric terminator; see http://partsregistry.org/Part:BBa_B0015 and http://partsregistry.org/Part:BBa_J61048) for more information. Gates were cloned within a pSB4A5 low copy plasmid ((*33*) pSC101 origin, 5 to 10 copies, iGEM registry accession number: pSB4A5), the low copy phagemid pWSK29 ((*34*), kindly provided by Prof. Sydney A. Kurshner, University of Georgia, USA, GenBank accession number: AF016889.1), or the CRIM integration vector (*35*).

All cloning PCR reactions were performed using the platinum Hi-Fi PCR supermix (Invitrogen, USA), using a 1 min. extension time per kilobase. Primers were purchased from IDT. All DNA assembly reactions were performed via Gibson one step isothermal assembly (*36*). Plasmid maps are shown in Appendix 3. Primers sequences are given in Appendix 4. DNA sequences have been deposited in Genbank (accession numbers: KC529324-KC529332).

1.1. *Dual controller plasmid*

The RAD module G8-C1 ((*5*), J64100 plasmid, ColE1 origin of replication, 50-70 copies, chloramphenicol resistance) containing the Bxb1 integrase under the control of pTET and Bxb1 RDF plus integrase under the control of pBAD was PCR amplified with primers JB424-425, removing the Bxb1 RDF/integrase cassette. The TP901 integrase was PCR amplified using primers JB422-423. This PCR product was ligated downstream of pBAD via Gibson assembly to generate the dual controller plasmid and sequence verified.

1.2. *Gate plasmids*

XOR

The pSB4A5 backbone containing the RBS-GFP-terminator cassette was PCR amplified using primers JB431 and JB434 to generate an open backbone with a 3' end BioBrick prefix on a 5' end GFP cassette. The XOR gate was amplified by PCR using primers G1004 (fwd BioBrick prefix) and JB435. XOR was ligated by Gibson assembly between the BioBrick prefix and the GFP cassette to generate pSB4A5_XOR_GFP.

AND

To generate pSB4A5_AND_GFP, the pSB4A5_XOR_GFP backbone was PCR amplified using primers JB459 and JB460 to remove the XOR logic register while conserving the input promoter, part of the TP901 recombination site, and the GFP cassette. The AND gate was PCR amplified with primers JB457 and JB458 and the two fragments were assembled and sequence verified.

NAND

To generate pSB4A5_NAND_GFP, the pSB4A5_XOR_GFP backbone was PCR amplified using primers JB470 and JB468 to remove the XOR logic register while conserving the input promoter, part of the TP901 recombination site, and the GFP cassette. The NAND gate was PCR amplified with primers JB457 and JB458 and the two fragments were assembled and sequence verified.

OR

For building pSB4A5_OR_GFP, the pSB4A5_AND_GFP backbone was PCR amplified using primers JB470 and JB 468 to remove the AND logic register while conserving the input promoter, part of the TP901 recombination site, and the GFP cassette. The OR gate was PCR amplified with primers JB466 and JB473 and the two fragments were assembled and sequence verified.

NOR

For building pSB4A5_NOR_GFP, the pSB4A5_AND_GFP backbone was PCR amplified using primers JB469 and JB 468 to remove the AND logic register while conserving the input promoter, part of the TP901 recombination site, and the GFP cassette. The NOR gate was PCR amplified with primers JB466 and JB483 and the two fragments were assembled and sequence verified.

XNOR

For building pSB4A5_XNOR_GFP, the pSB4A5_XOR_GFP backbone was PCR amplified using primers JB470 and JB468 to remove the XOR logic register while conserving the input promoter, part of the TP901 recombination site, and the GFP cassette. The XNOR gate was PCR amplified with primers JB472 and JB473 and the two fragments were assembled and sequence verified.

pIT3_Phi21_AND_GFP, piT3_Phi21_AND_GFP (plasmid for chromosomal integration).

The pIT3_phi21_Kan vector was PCR amplified using primers JB518 and JB519. pSB4A5_AND_GFP and pSB4A5_XNOR_GFP were PCR amplified using primers JB520 and JB521, and the two fragments were assembled and sequence verified.

pWSK29mod_AND (plasmid for M13 packaging).

To clone the gates into the phagemid pWSK29 (*34*), the phagemid backbone was amplified by PCR using primers JB551 and JB552, eliminating the lacZalpha fragment and adding the BioBrick prefix and suffix in a single PCR reaction. The input promoter, logic element, and GFP sequences from pSB4A5_AND_GFP were amplified in a second PCR reaction using primers JB549 and JB550. The two DNA strands were ligated together via Gibson assembly and sequence verified.

1.3. *Measurement plasmids*

Dual controller pTET_GFP

The dual controller plasmid was PCR amplified with primers JB510 and JB511, removing the Bxb1 integrase gene and its RBS. The GFP cassette (RBS plus GFP) was PCR amplified from pSB4A5_AND_GFP by using primers JB508 and JB509. This PCR product was ligated downstream of pTET in the above vector via Gibson assembly to generate a dual controller measurement plasmid in which Bxb1 is replaced by the GFP cassette used in the logic gates.

Dual controller pBAD_GFP

The dual controller plasmid was PCR amplified with primers JB514 and JB515, removing the TP901 integrase gene and its RBS. The GFP cassette was PCR amplified from pSB4A5_AND_GFP by using primers JB512 and JB513. This PCR product was ligated downstream of pTET in the above vector via Gibson assembly to generate a dual controller measurement plasmid in which TP901 is replaced by the GFP cassette used in the logic gates.

2. Cell Culture, data collection, and analysis.

Plasmids were transformed via heat-shock in chemically competent *E. coli* DH5alphaZ1 *(32)* and plated on LB agar plates containing the appropriate antibiotics. For main Figures 2-4 the controller plasmid was co-transformed with the pSB4A5_Gate plasmid. For the sequential input logic experiment, the controller plasmid was transformed in cells containing a Phi21 chromosomally integrated logic gate and harboring a kanamycin resistance cassette. Antibiotics were used at the following concentrations: carbenicillin (25ug/ml), kanamycin (30ug/ml) and chloramphenicol (25ug/ml) (all from Sigma). Cells containing chromosomally integrated gates were grown with 5ug/ml of kanamycin.

For each experiment, and unless otherwise stated, after overnight incubation of the plate, three colonies were separately inoculated in Azure Hi-Def media (Teknova, Hollister, USA) with glycerol (0.4%, from Fisher Scientific) added as a carbon source and appropriate antibiotics and grown for approximatively 18 hours to obtain starter cultures. L-arabinose (ara) was obtained from Calbiochem. Anhydrotetracycline (aTc) was obtained from Sigma.

2.1. Buffer gate operation

Bxb1 integrase and excisionase were controlled via aTc and arabinose inducible promoters, respectively, on pSB3k1 plasmid (p15A origin; 15-20 copies). DNA data register was on pSB4A5 plasmid (*(32)*, pSC101 origin; 5 copies; Genbank:JQ929581). The experiment was performed in *E. coli* DH5alpha (tetR-) cultured at 37C in supplemented M9 medium [M9 salt (Sigma), 1 mM thiamine hydrochloride(Sigma), 0.2% casamino acid (Across Organics), 0.1 M MgSO4 (EMD reagents), 0.5 M CaCl2 (Sigma) with glycerol (0.4%, Fisher Scientific) added as a carbon sources], 25 ug/ml carbenicillin and 50 ug/ml kanamycin. L-arabinose was used at a final concentration 0.1% w/v concentration. For each duty cycle, cultures were diluted 1:1000 in media with inducer, grown overnight, then diluted 1:1000 in media without inducer and grown over night. Results are presented in figure S3.

2.2. Dual control signal transfer functions.

To generate the dual control signal transfer functions presented in Figure 2, cells from the overnight starter culture were diluted 1:5000, induced with different concentrations and combinations of inducers, and grown in Azure Hi-Def media for 18H at 37C. Just before measurement, the resulting saturated cultures were diluted 1:20 in PBS. Samples were then analyzed on a Wallac Victor3 multi-well fluorimeter (Perkin Elmer). Absorbance at 600 and (AB600) and GFP intensity were measured (600 nm absorbance filter, 0.1 second counting time for AB; 485 nm excitation filter, 525 nm emission filter for GFP). Media background was substracted from AB600 and GFP values, and AB600 values obtained from the plate reader were converted to optical density (OD) by using the equation : OD600 = ((AB600 - 0.06)*3.11)- 0.0158; obtained from calibration (see also: http://openwetware.org/wiki/Endy:Victor3_absorbance_labels for more details). Average OD600 in the measured samples were between ~0.2-0.3, and we did not observe correlations between OD and GFP levels. For each well, the GFP value was divided by the OD600 value to correct for differences in cell density. GFP/OD were plotted using the MATLAB imagesc function. Numerical values and standard deviations for OD and GFP measurements are available in appendices 1 and 2 of the SOM.

2.3. Flow cytometry

Flow cytometry acquisition was performed at the Stanford Shared FACS Facility (SSFF) using a BD-Bioscience-LSR II cytometer (BD-Bioscience, San Jose, CA) coupled with a high-throughput sampler. 30,000 cells were collected for each data point. All acquisitions were performed using the same machine and settings. Just before measurement, cultures were diluted 1:100 in ice cold PBS. Flow cytometry data were analyzed using the FlowJo software (Treestar inc., Ashland, USA). Figure S5 details the different analyses that were performed.

For single cell measurements in Figure 2, arabinose was used at a final 1% w/v concentration and aTc was used at a final concentration of 200 ng/ml. Measurements of the percentage of cells flipping were performed using a common fluorescence intensity threshold for all gates as represented by the red line.

2.4. Transfer functions and switching range in response to individual controllers.

Transfer functions for individual integrases were measured using cells containing the dual controller plasmid and a Bxb1 or a TP901 BP register encoded on pSB4A5 ((*5)* and plasmid map K*)*.

For experiments presented in Figures 3 and 4, cells from the starter cultures were diluted 1:5000 in different inducers concentrations and grown for 20 hours at 30C. For AND and NAND gates, measurement with one inducer were done in the presence of saturating concentration of the other. For each experimental replicate, the measurement plasmids pTET-GFP and pBAD-GFP were run in parallel.

For Figure 4, gate-specific thresholds were defined for each logic function. Histograms displaying fluorescence intensities of GFP were generated and the cell population in the ON state was gated. We used the gate specific gating (fig. S7) to quantify the fraction of cells in ON state, from which we determined the gates switching ranges (fig. S8). To quantify fluorescence intensity, we measured the median fluorescence intensity of the whole population using FlowJo.

2.5. Digitization and digital error rate calculation

For Figure 3CD, controllers and logic gates were gated manually to minimize the probability of scoring a cell in the OFF state as ON, and a cell in the ON state as OFF. We added the two numbers to obtain a digitization error rate.

2.6. Fold changes calculations for gates and promoters.

Whole population median fluorescence intensities for different gates were extracted from flow-cytometry data at various inducer concentrations (fig. S8). For Figure 4, all fluorescence intensity values were normalized for each gate and controllers to equal a value of 1 in the abscence of inducer. As such, normalized values correspond to the fold change in fluorescence intensity versus a base fluorescence intensity for each gate or controller. For each experiment the control signal vectors used to quantify controller activity were run in parallel with the gates. Calculations of fold change were made independently for each experiment. Experiments were then averaged, standard deviation calculated, and data plotted using MATLAB (Mathworks, Natic, USA). Results are the average of three independent experiments +/- SD. Non-normalized plots of the GFP values corresponding to the respective gate outputs versus GFP levels corresponding to the control signals are provided in figure S10.

2.5. Single-cell dynamic ranges and fold changes measurements.

The dynamic ranges of logic gate outputs and of the control signals were measured across a common gate switching range, using the cytometry gating method presented in figure S7. Single cell fluorescence intensity of the OFF state for AND, OR and XOR was determined by measuring the median fluorescence intensity for the fraction of the cell population gated for the OFF state at the *lower* inducer concentration of the switching range (0.2 ng/ml for pTET and 1E-4% for pBAD). Single cell fluorescence intensity of the OFF state for NAND, NOR and XNOR was determined a similar manner but at the *higher* inducer concentration of the switching range (5 ng/ml for pTET and 1E-2% for pBAD). Single cell fluorescence intensity of the ON state for AND, OR and XOR was determined by measuring the median fluorescence intensity for the fraction of cell population gated for the ON state, at the *higher* inducer concentration of the switching range. Single cell fluorescence intensity of the ON state for NAND, NOR and XNOR was determined in a similar manner but at the the *lower* inducer concentration of the switching range. Results are presented in figure S9.

2.6. Sequential logic experiment.

Logic gates used in the sequential logic experiment were integrated into *E. coli* DH5alphaZ1 chromosome (*32)* using a modified version of the CRIM system (*34)*, Sherwin, St-Pierre unpublished results), using the phi21 integrase integration sites. Sequential input logic experiments were performed at 37C with 1% w/v arabinose and 200 ng/ml aTc. For storage mode, induced cultures were washed and diluted 1:2000 in media without inducer, in order to achieve about 10 generations per day (log2 2000 = 10.96) . Results are presented in figure S11.

2.7. Cell-cell communication of DNA encoding intermediate logic states

All experiments for phage-based logic messaging were conducted in LB liquid culture using *E. coli* strain DH5alphaZ1, F^+. This F^+ strain was created by mating DH5alphaZ1 with XL1-Blue. For all experiments, infected sender cells were prepared by co-transforming chemically-competent cells with M13K07 phagemid in addition to the messaging phagemid, pWSK29mod_AND. Receiver cells were prepared by transforming chemically-competent cells with the dual-controller plasmid via heat shock. Overnight cultures of sender and receiver cells were diluted 100x into fresh media with appropriate antibiotics (sender cells were grown with 50 μg/mL kanamycin and 50 μg/mL carbenicillin; receiver cells were grown with 10 μg/mL tetracycline and 25 μg/mL chloramphenicol). The diluted cultures were returned to log phase ($OD_{600} \approx 0.7$) by incubation with shaking at 37C. From these log phase cultures we prepared co-cultures containing a 50x dilution of both sender and receiver cells in a total of 5 mL fresh media without added antibiotic. Co-cultures were incubated at 37C with shaking for 5 hours and then diluted 100x into fresh media containing 50 μg/mL carbenicillin and 25 μg/mL chloramphenicol, in one of four induction states: (1) no

inducers; (2) anhydrous tetracycline only; (3) arabinose only; and, (4) both anhydrous tetracycline and arabinose. Inducer levels were set at 0.1% w/v arabinose and 200ng/ml anhydrous tetracycline. These cultures were grown in 96-well plate format at 37C for 16 hours. For each messaging phagemid, three colonies were tested, and inducer states for each colony were tested in triplicate. After incubation, a 200 µl aliquot of each culture was transferred into a flat-bottomed 96-well plate and OD_{600} and GFP fluorescence of each culture was measured on a Wallac Victor3 multi-well fluorimeter (Perkin Elmer). Results are presented in figure S12.

2.8. Measurement of recombination kinetics.

Gate switching kinetics via plate reader measurements

Three colonies containing the AND or the XOR gate with the dual controller plasmid or containing the pTET or pBAD measurement plasmid only were inoculated in Azure Hi-Def media and grown overnight. On the next day, these starter cultures were diluted 1:100 and grown in Azure Hi-Def media until they reach 0.3 OD. We transferred 200 µl from each cultures into a well on a flat-bottomed 96 well plate, with different combinations of inducers: for XOR, (i) no inducers, (ii) arabinose at 0.1% w/v, (iii) aTc at 200ng/ml, and for AND, (i) no inducers, (ii) arabinose plus aTc at the previous concentrations. Measurement plasmids were run in parallel with the same inducer concentrations. We incubated the plate in a Wallac Victor3 multiwell fluorimeter at 37C and assayed the samples with an automatically repeating protocol of absorbance measurements (600 nm absorbance filter, 0.1 second counting time), fluorescence measurements (485 nm excitation filter, 525 nm emission filter, 0.1 second measurement time), and shaking (10 minutes interval between measurements with linear type). Data were plotted using a custom MATLAB script (figure S13).

Recombination kinetics measured via flow cytometry.

Cells were co-transformed with: (i) a pSB4A5-BP_GFP plasmid (containing a data register with Bxb1 or TP901 BP sites flanking a constitutive promoter and producing GFP upon inversion, plasmid maps L and M) and (ii) pBAD-Bxb1-Set Generator ((*5)*, Genbank:JQ929583) or pBAD-TP901 (same as previous but Bxb1 gene replaced by TP901, plasmid map J). Colonies were inoculated overnight and the day after, starter cultures were diluted in 30ml flasks in supplemented M9 media and grown at 37C. When OD reached 0.4, cells were split in two cultures, one which was induced with 0.1% arabinose, the other being left un-induced. At each time-point, a 1 ml aliquot was taken and immediately fixed by addition of paraformaldehyde (PFA) (Electron Microscopy Sciences #15714-S) to a final concentration of 1% followed by storage at 4C. The non-induced cells were also fixed in a similar manner. Samples were diluted 1:100 in PBS prior to flow cytometry (fig. S13C).

Minimum control signal duration experiments

Starter culture from cells containing pBAD-Bxb1-Set-Generator (JQ929583) and the pSB4A5_BP register (JQ929581) were diluted in 30ml flasks in supplemented M9 media and grown at 37C. When OD reached 0.4, cells were split into two cultures, one which was induced with 0.1% arabinose, the other left un-induced. Five minutes before each time point, a 1ml aliquot was taken and cells were immediately spun and washed twice with fresh media that did not contain arabinose. Washed cells were diluted 1:1000 in fresh media and grown overnight at 37C. Samples were diluted 1:100 in PBS prior to being analyzed flow cytometry (fig. S13D).

Single cell time lapse microscopy

Cells containing the pBAD-Bxb1-Set-Generator ((*5),* JQ929583) and the pSB4A5_BP-register (JQ929581) were grown to exponential phase in supplemented M9 (OD~0.3) and spread on M9/glycerol 2% agarose pads supplemented with 0.5% arabinose to induce expression of the Bxb1 integrase cassette. We immediately incubated the cells in a microscope heating chamber set to 37C, taking phase contrast, GFP and RFP fluorescence images every 5 min at a 100X magnification (see Supplementary Movie 1).

3. Phenomenological model of Boolean integrase logic gates

We fit the response curves of individual DNA registers (with inducer concentration as an input and probability of being in LR state as an output) to Hill functions below (fig. S4).

For the arabinose inducible TP901 DNA register,

$$LR_{TP} = f(ara) = \frac{ara^2}{ara^2 + 0.003^2} \quad \text{(A)}.$$

For the aTc inducible Bxb1 DNA register,

$$LR_{BX} = g(ATc) = \frac{ATc^2}{ATc^2 + 1.5^2} \quad \text{(B)}.$$

For all two-input logic gates, we assume no cross talk between Bxb1 and TP901 integrase. Thus, the probability of recombining Bxb1 attB/attP is independent of TP901 integrase inducer level, and vice versa.

An AND gate is in an ON state when both Bxb1 and TP901 DNA register are in an LR state. Under no-cross talk assumption, the probability of having an AND gate in an ON state is thus the product of the probability of having the Bxb1 DNA register in a LR state and the

$$ON_{AND} = AB.$$

probability of having the TP901 DNA register in an LR state, i.e.,Similarly, a NOR gate is in an ON state when both Bxb1 and TP901 sites are in BP state. Thus, the probability of having a NOR gate in an ON state is thus the product of the probability of having the Bxb1 latch in a BP state and the probability of having the TP901 DNA register in a BP state, i.e.,

$$ON_{NOR} = (1 - A)(1 - B).$$

An OR gate is in an ON state when either Bxb1 or TP901 DNA registers are in LR state. Thus, the probability of having an OR gate in an ON state is determined by the DNA register, Bxb1 or TP901, that is more likely to be in an LR state, i.e.,

$$ON_{OR} = \max(A, B).$$

Similarly, a NAND gate is in an ON state when either Bxb1 or TP901 sites are in BP state. Thus, the probability of having a NAND gate in an ON state is determined by the DNA register, Bxb1 or TP901, that is more likely to be in a BP state, i.e.,

$$ON_{NAND} = \max\big((1 - A), (1 - B)\big).$$

An XOR gate is in an ON state in two possible scenarios. The first scenario is when Bxb1 DNA register is in a BP state and TP901 DNA register is in an LR state. Under non-crosstalk assumption, the probability of this scenario is simply the product of the probability of having a BP state Bxb1 DNA register and the probability of an LR state TP901 DNA register, i.e., A(1-B). The second scenario is when Bxb1 DNA register is in an LR state and that Bxb1 DNA register is in a BP state. Under non-crosstalk assumption, this probability would be (1-A)B. In total, the probability of being in either scenarios is:

$$ON_{XOR} = \max(A(1 - B), (1 - A)B).$$

Similarly, an XNOR gate is in an ON state in two possible scenarios: when both Bxb1 and TP901 DNA registers are in LR state or when both DNA register are in BP state. Given non-crosstalk assumption, the former has probability AB while the latter has probability (1-A)(1-B). Thus, the probability of having ON XNOR becomes:

$$ON_{XNOR} = \max\big(AB, (1 - A)(1 - B)\big).$$

fig. S1:

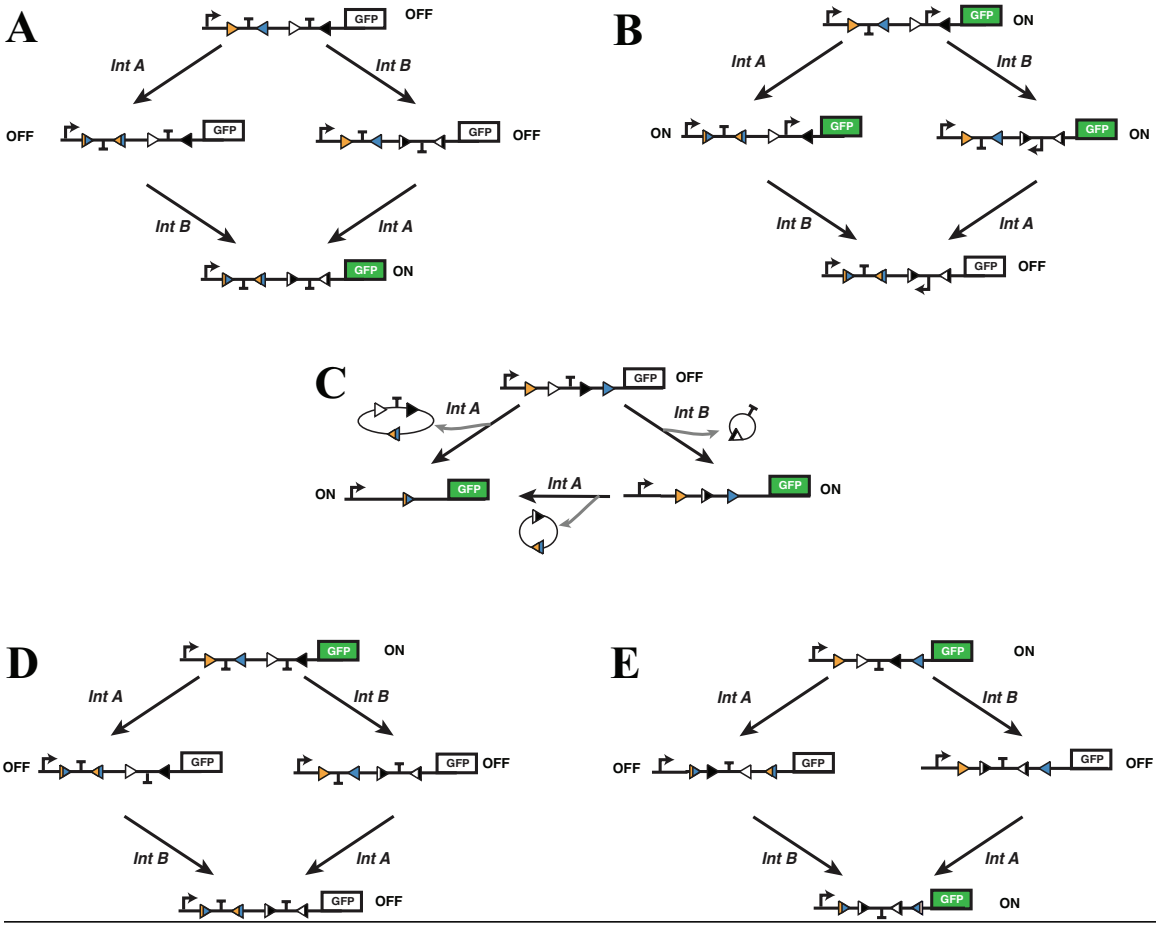
A
GFP
OFF
Int A
Int B
OFF
GFP
GFP
OFF
Int B
Int A
GFP
ON
B
GFP
ON
Int A
Int B
ON
GFP
GFP
ON
Int B
Int A
GFP
OFF
C
GFP
OFF
Int A
Int B
ON
GFP
Int A
GFP
ON
D
GFP
ON
Int A
Int B
OFF
GFP
GFP
OFF
Int B
Int A
GFP
OFF
E
GFP
ON
Int A
Int B
OFF
GFP
GFP
OFF
Int B
Int A
GFP
ON

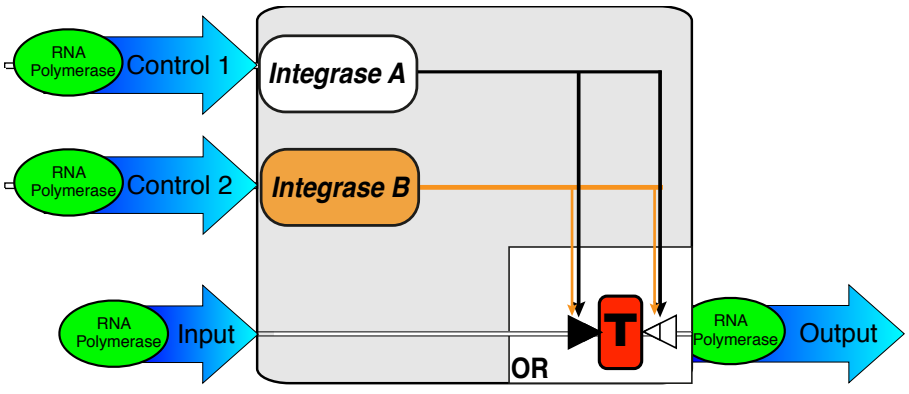
F
RNA Polymerase
Control 1
Integrase A
RNA Polymerase
Control 2
Integrase B
RNA Polymerase
Input
T
OR
RNA Polymerase
Output

figure S1: Detailed gates state diagram: (A) AND, **(B)** NAND, **(C)** OR, **(D)** NOR, and **(E)** XNOR. Logic gates consist of: (i) a constitutive input promoter (P7-modular promoters library (44)) (ii) a logic element made of a specific arrangement of recombination sites and transcription regulatory sequences controlling the flow of RNA polymerase through the gate. For AND and NOR gates, we used a double terminator (BBa_B0015) flanked by TP901 target sites (blue and orange) and a Rrnp T1 terminator (BBa_J61048) flanked by Bxb1 target sites (black and white). For NAND gate, B0015 is flanked by TP901 sites and P7 promoter is flanked by Bxb1 sites. For OR, XOR and XNOR, we used the B0015 terminator. (iii) finally downstream of the logic element we cloned superfolder GFP *(31)*BBa_I746916) under translational control of a measured strong RBS (JBEI-RBS, Biofab pilot C-dog project http://biofab.org/data) to record gate outputs **(F)** An alternative architecture OR gate in which two copies of the same integrase are controlled by two distinct signals.

fig. S2:

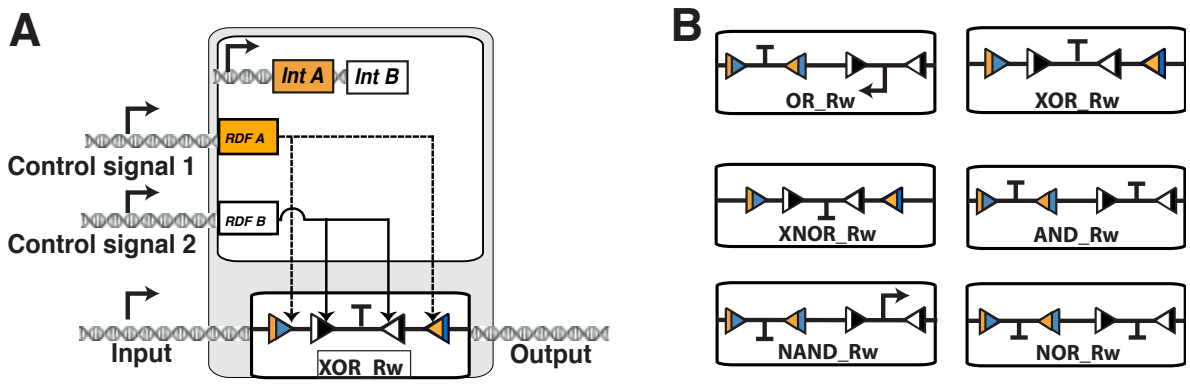

figure S2: Rewritable Boolean integrase logic gates. (A) A constitutive promoter expresses both integrases, Int A and Int B. Control signals drive expression of recombination directionality factors (RDFs); BP sites used in permanent gates are replaced by LR sites recognized by integrase/RDFs complexes, producing rewritable (Rw) logic gates (see Bonnet et al., 2012 for details (*5)*). **(B)** Rewritable logic element schematics for all gates presented in the main text.

fig. S3:

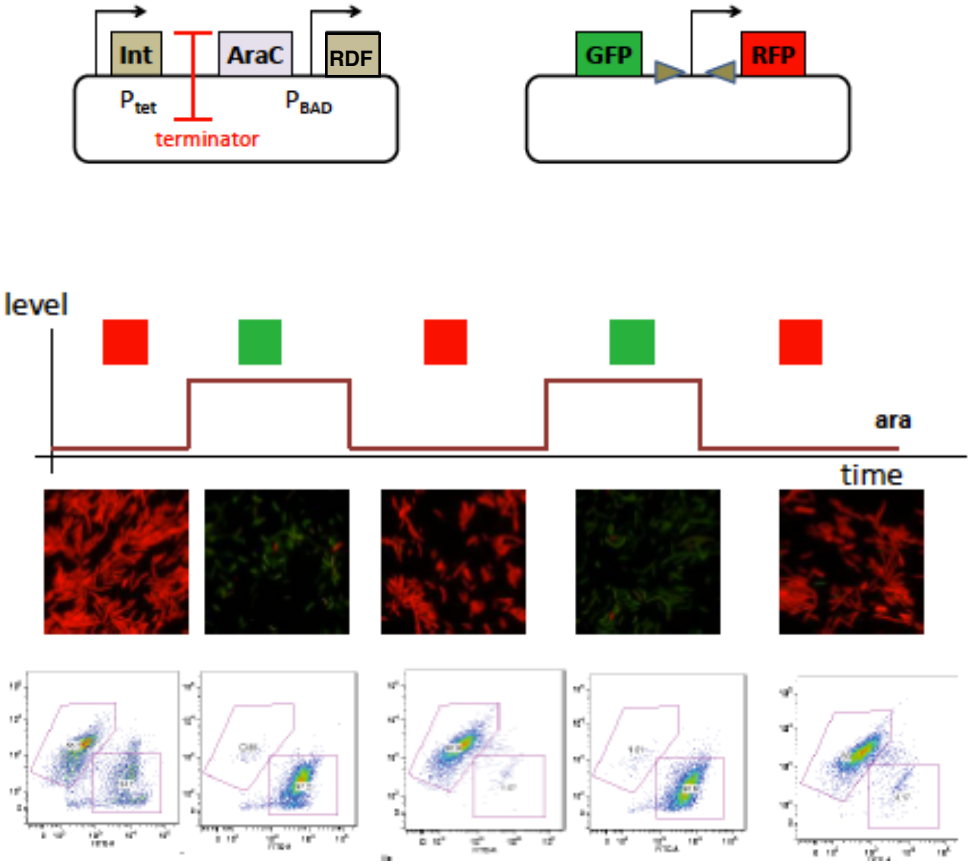

figure S3: Demonstration of a rewritable buffer gate. (A) Schematic of the constructs used in this experiment. Integrase expression is under the control of the pTET promoter, while RDF expression is controlled by pBAD. The target plasmid contains a promoter flanked by BP sites. The BP state expresses GFP while the LR state expresses RFP. **(B)** Rewritable Buffer gate operation. Cells were exposed to pulses of arabinose (overnight cultures) to vary expression of the RDF while integrase expression was made constitutive by using a DH5alpha strain lacking the Tet repressor. Expression of the RDF drives cells to the BP state with near-completion efficiency. In the absence of arabinose (overnight cultures), cells relax back to the LR state via integrase mediated recombination. The system can be cycled multiple times.

Fig S4:

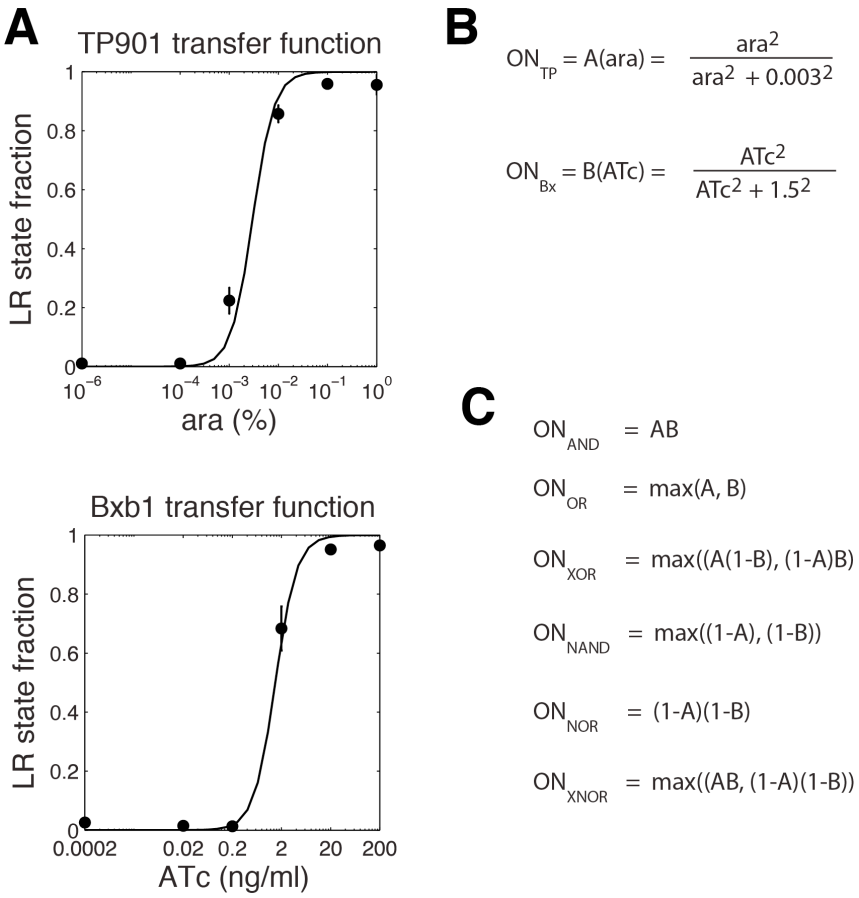

figure S4: Abstracted models for logic element switching. (A) Experimentally measured transfer functions for the TP901-1 and Bxb1 integrases. The fraction of cells flipping from a BP to LR state was measured as a function of arabinose (ara) or anhydrotetracycline (aTc) concentrations **(B)** Hill equation parameters for each individual integrase were obtained by fitting experimental data. **(C)** The equations obtained in (B) were combined into gate-specific functions for each distinct Boolean operation and used to predict two controller transfer functions shown in Main Figure 2.

fig. S5

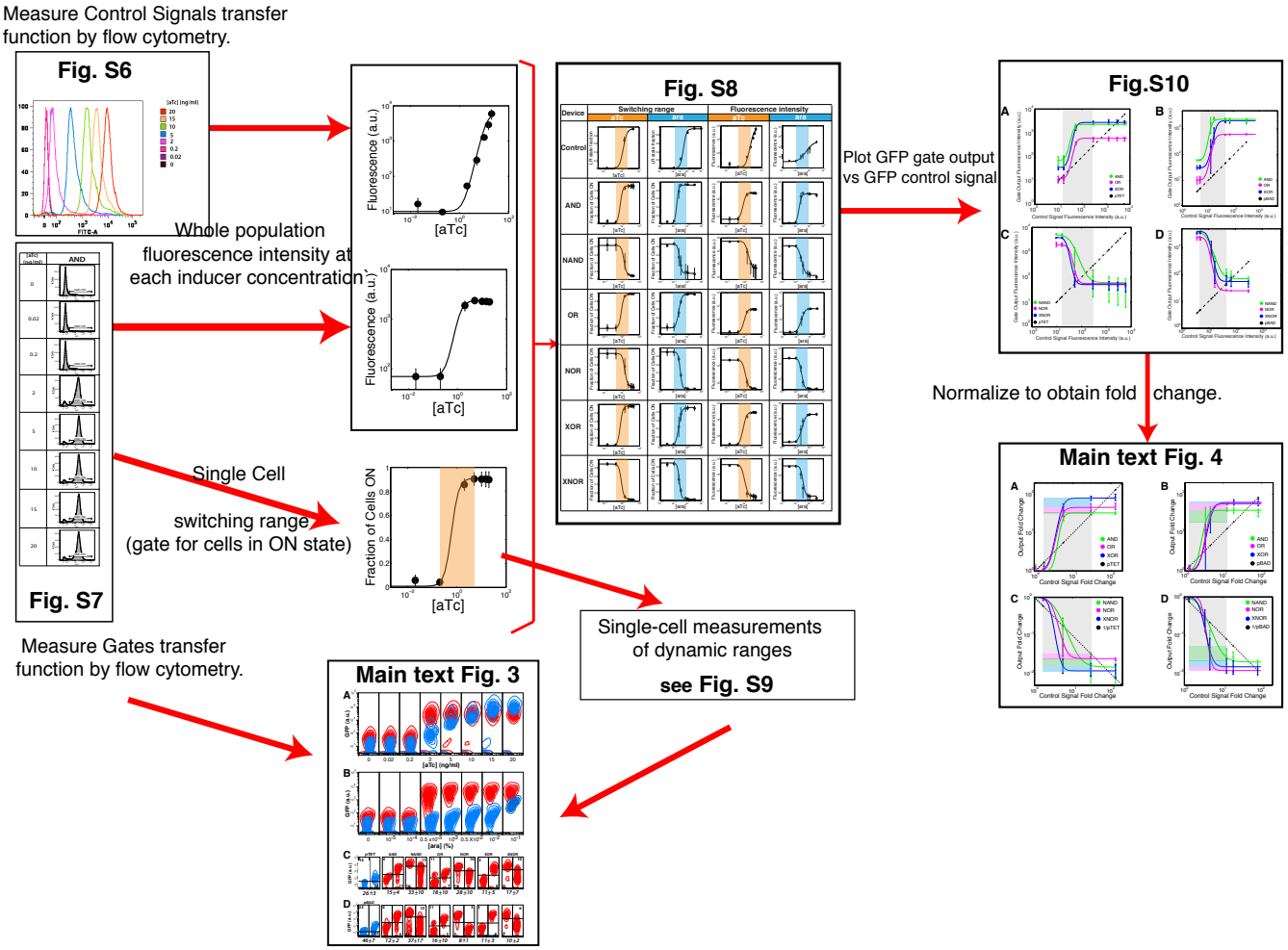

figure S5: Schema describing how transfer functions, dynamic ranges, and fold changes were measured and processed to produce various figures. After measuring transfer functions for both control signals (fig. S6) and the logic gates by flow cytometry (fig. S7), whole population fluorescence intensity was measured at each inducer concentration. An example is depicted here with an AND gate and the pTET controller. The resulting transfer functions were plotted with single cell switching transfer functions in fig. S8. The flow cytometry data were used to determine the digital error rate for the gates and the promoters (Figure 3, main text). The raw, whole population GFP output from the gates was then plotted against the GFP output of the control signal at each inducer concentration (fig. S10). These data were normalized and plotted to obtain the relative gate output fold change versus control signal fold changes presented in Main Figure 4. Single cell measurements of dynamic ranges and fold changes are displayed in more detail in fig. S9.

fig. S6

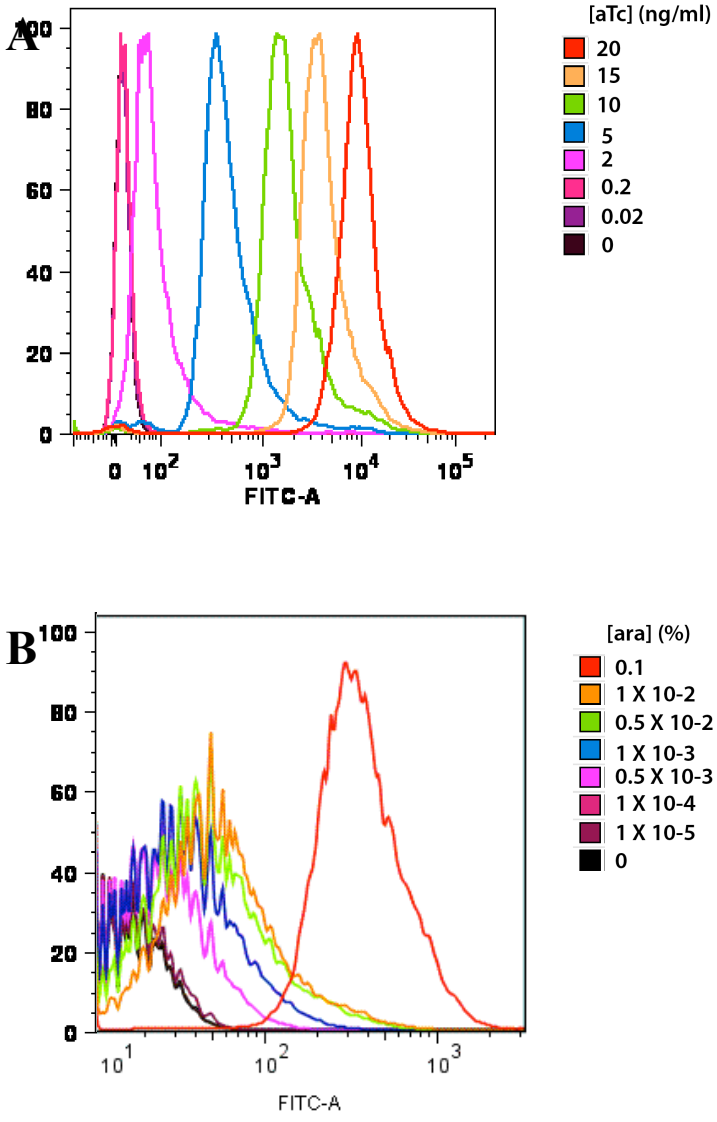

figure S6: Raw flow cytometry data for the control signals transfer functions presented in Fig. 3 and fig. S8. (A) pTET and **(B)** pBAD, using the measurement plasmids (plasmid maps, B-C).

figure S7

A

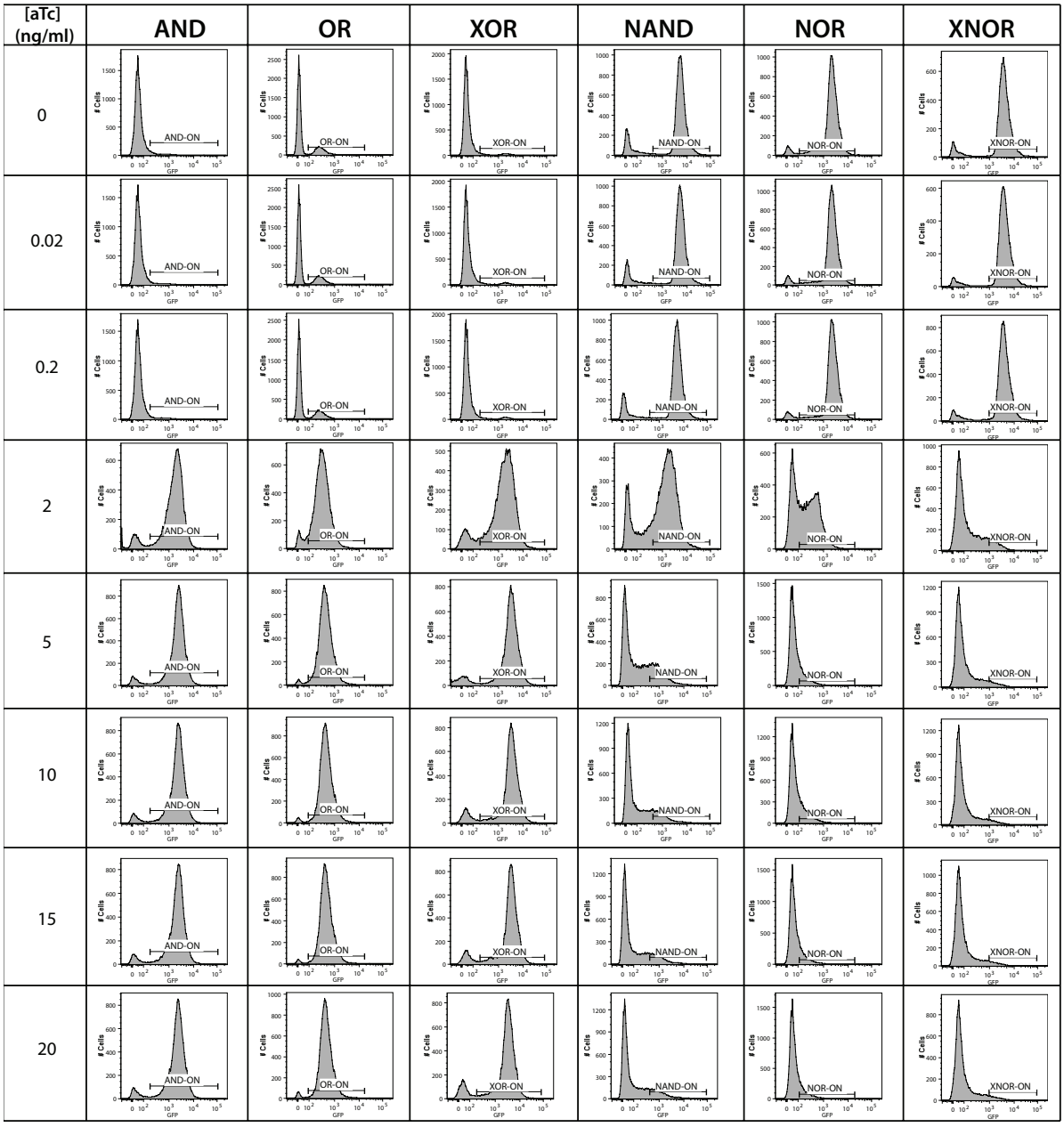
[aTc] (ng/ml)
AND
OR
XOR
NAND
NOR
XNOR
0
0.02
0.2
2
5
10
15
20
AND-ON
OR-ON
XOR-ON
NAND-ON
NOR-ON
XNOR-ON
Cells
GFP

figure S7 (continued)

B

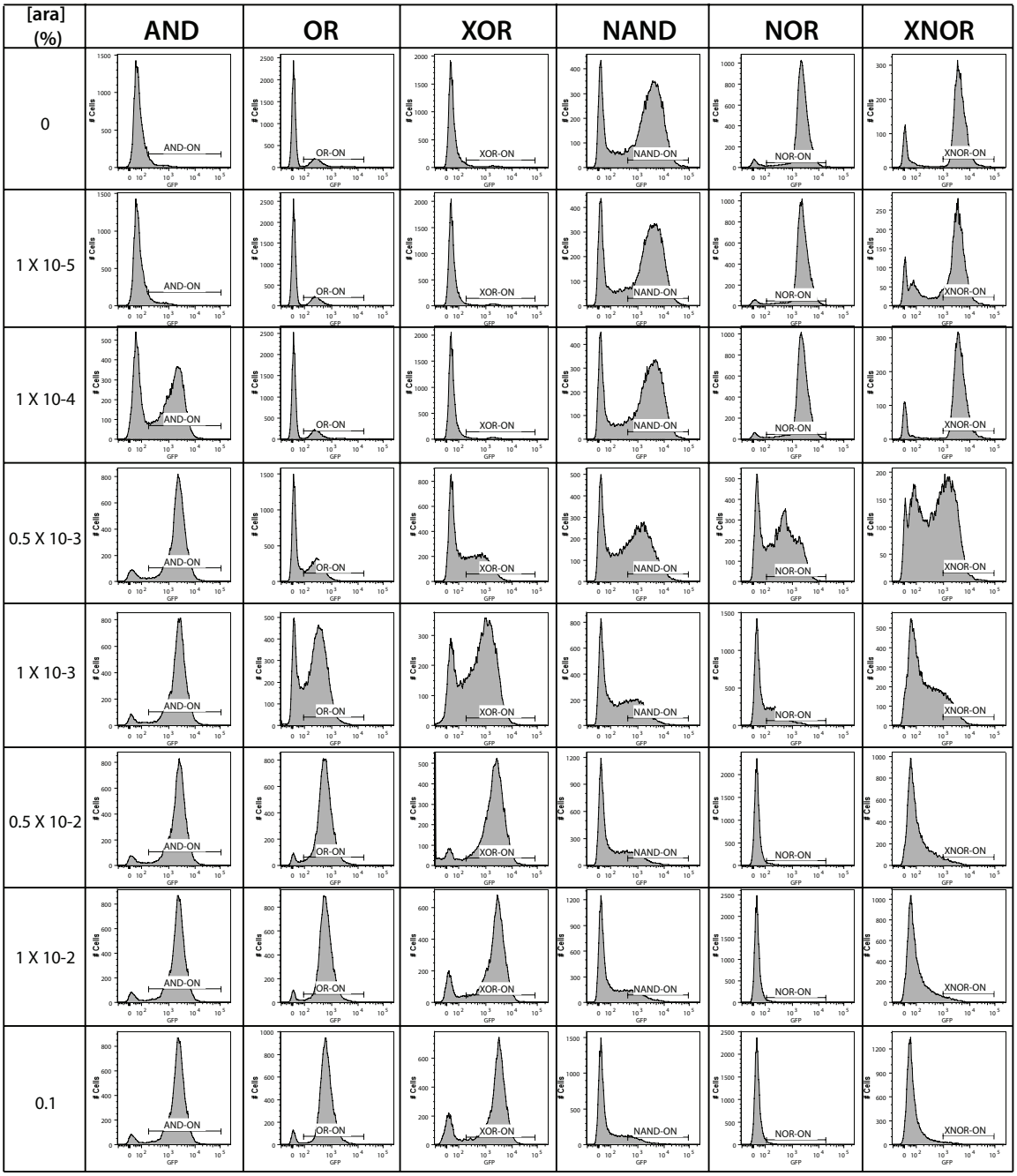

figure S7: Example of raw flow cytometry data and the gating method used to generate the data presented in fig. S8, S9, S10 and Main Text Fig. 4. (A) Response of gates to aTc regulated controller. **(B)** Response of gates to arabinose regulated controller. For the AND and NAND gates, measurement for a particular inducer was done in the presence of saturating concentrations of the other inducer.

fig. S8

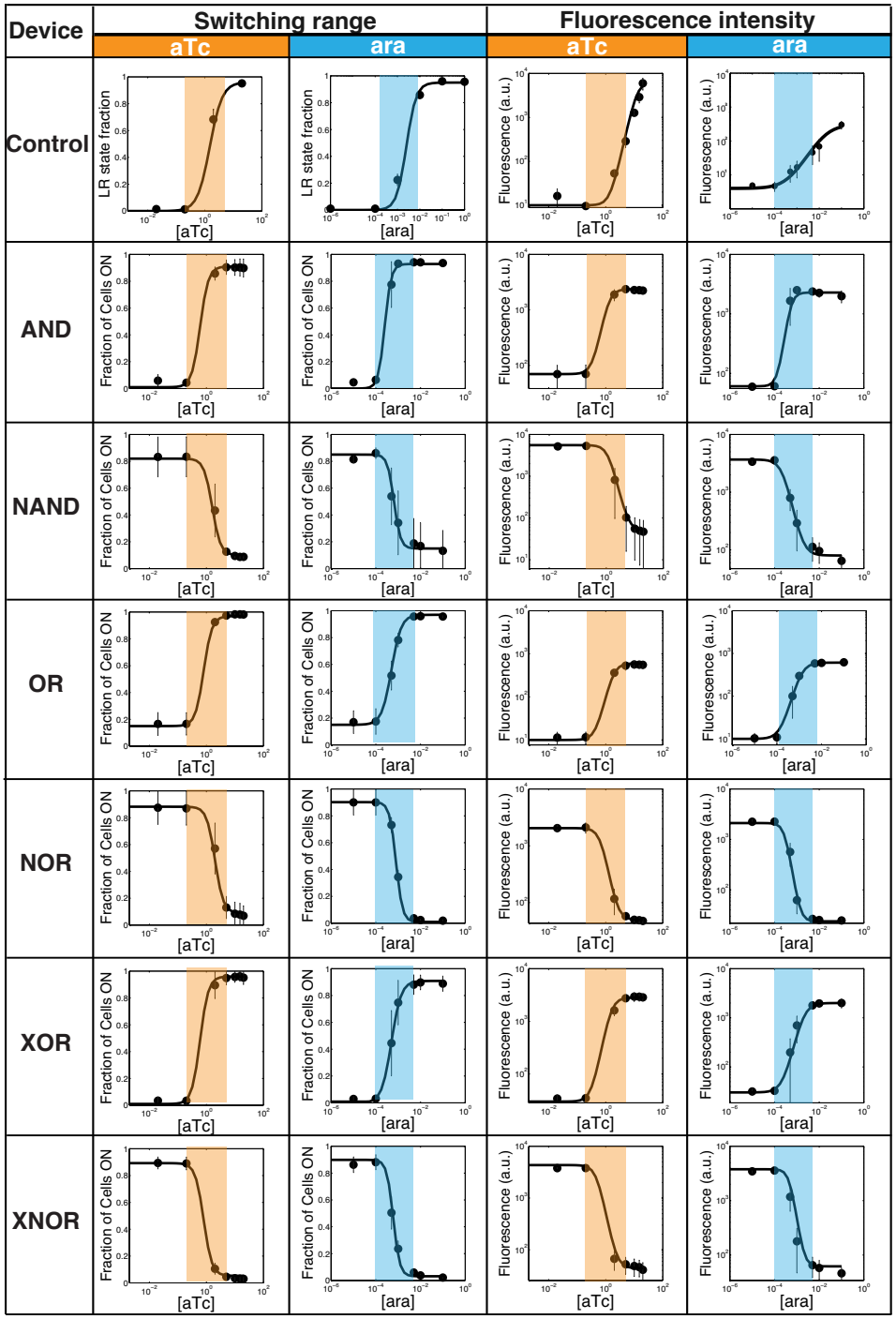

figure S8: Quantitative measurement of gates response to individual control signals. The common control switching range (shaded areas) was measured as the range of inducer concentration required to switch between less than 10% and more than 80% of cells in an ON state. The "control" graphs in the switching range section represent the transfer functions of individual Bxb1 (aTc) and TP901 integrase (ara) buffer gates (see also fig. S4). The "control" graphs in the fluorescence intensity section represent the transfer functions of individual pTET (aTc) and pBAD (ara) promoters performed using the measurement plasmids. Variation in fluorescence intensity in response to varying concentrations of individual inducers for each gate was plotted as the median intensity of the whole population at each inducer concentration. Results are the average of three independent experiments +/- SD.

fig. S9

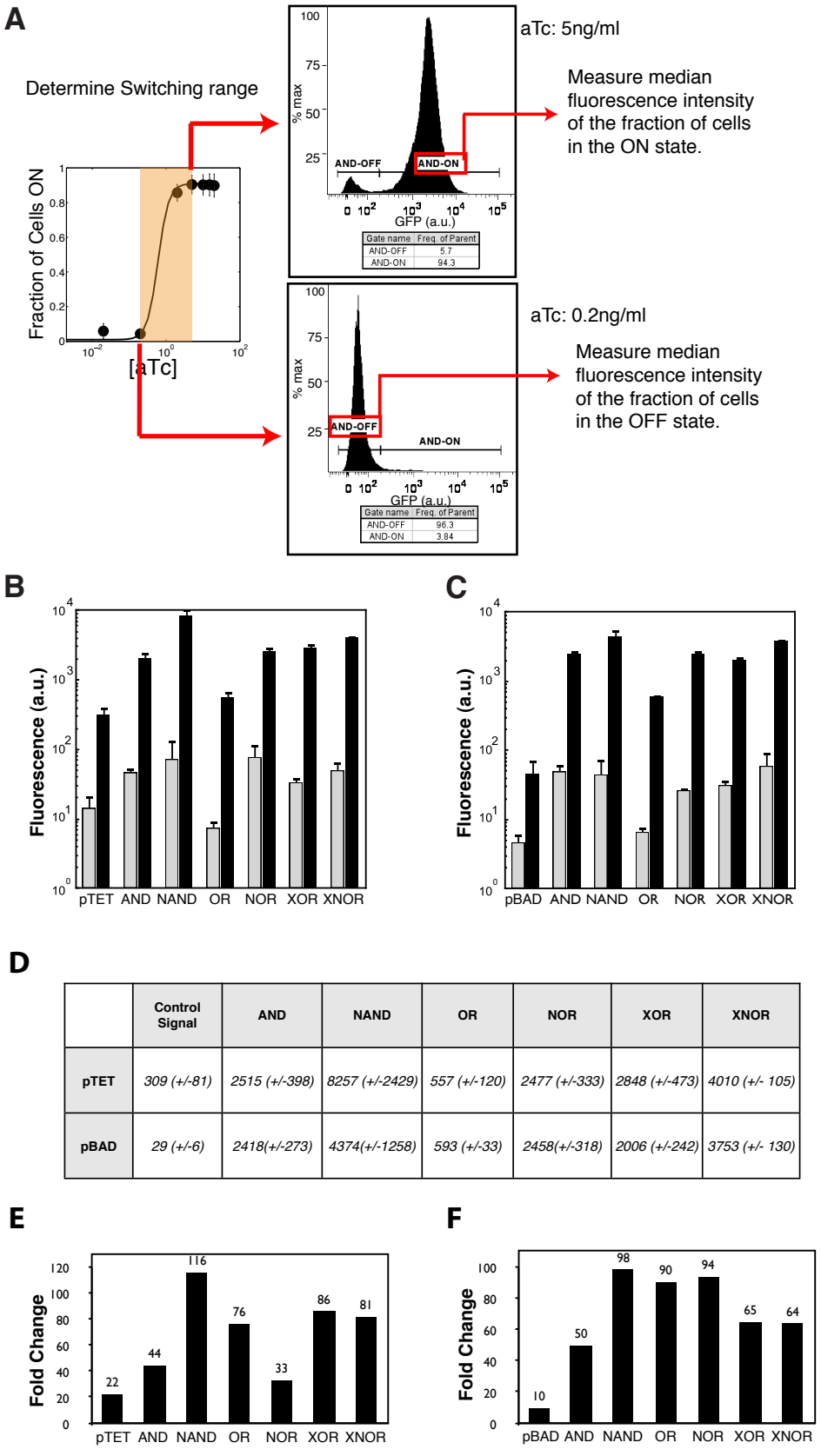

D

	Control Signal	AND	NAND	OR	NOR	XOR	XNOR
pTET	*309 (+/-81)*	*2515 (+/-398)*	*8257 (+/-2429)*	*557 (+/-120)*	*2477 (+/-333)*	*2848 (+/-473)*	*4010 (+/- 105)*
pBAD	*29 (+/-6)*	*2418(+/-273)*	*4374(+/-1258)*	*593 (+/-33)*	*2458(+/-318)*	*2006 (+/-242)*	*3753 (+/- 130)*

figure S9: (previous page) Gate dynamic ranges and control signal amplification. (A) Method for determining the gate dynamic ranges at the single cell level: example with the AND gate response to aTc. The dynamic ranges of the logic gates and of the control signals were measured across the common gate switching ranges, using the cytometry gating method presented in fig. S7. Single cell fluorescence intensity of the OFF state for AND, OR and XOR was determined by measuring the median fluorescence intensity for the fraction of the cell population gated for the OFF state at the *lower* inducer concentration of the switching range (0.2 ng/ml for pTET and 1E-4% for pBAD). Single cell fluorescence intensity of the OFF state for NAND, NOR and XNOR was determined a similar manner but at the *higher* inducer concentration of the switching range (5 ng/ml for pTET and 1E-2% for pBAD). Single cell fluorescence intensity of the ON state for AND, OR and XOR was determined by measuring the median fluorescence intensity for the fraction of cell population gated for the ON state, at the *higher* inducer concentration of the switching range. Single cell fluorescence intensity of the ON state for NAND, NOR and XNOR was determined in a similar manner but at the the *lower* inducer concentration of the switching range. **(B)** Dynamic range of the gates in response to pTET and **(C)** Dynamic range of the gates in response to pBAD. Gray bars: OFF state. Black bars: ON state. Results are the average of 3 independent experiments +/- SD. **(D)** Differences in fluorescence intensity (arbitrary units) between the ON and OFF state for each gate, compared to the control signals, in response to individual inducers. Values are presented +/- SD. **(E-F)** Absolute values of the fold change in logic gate outputs between the ON and OFF states in response to pTET (E**)** or pBAD (F**)**, determined from data in (B) and (C).

fig. S10:

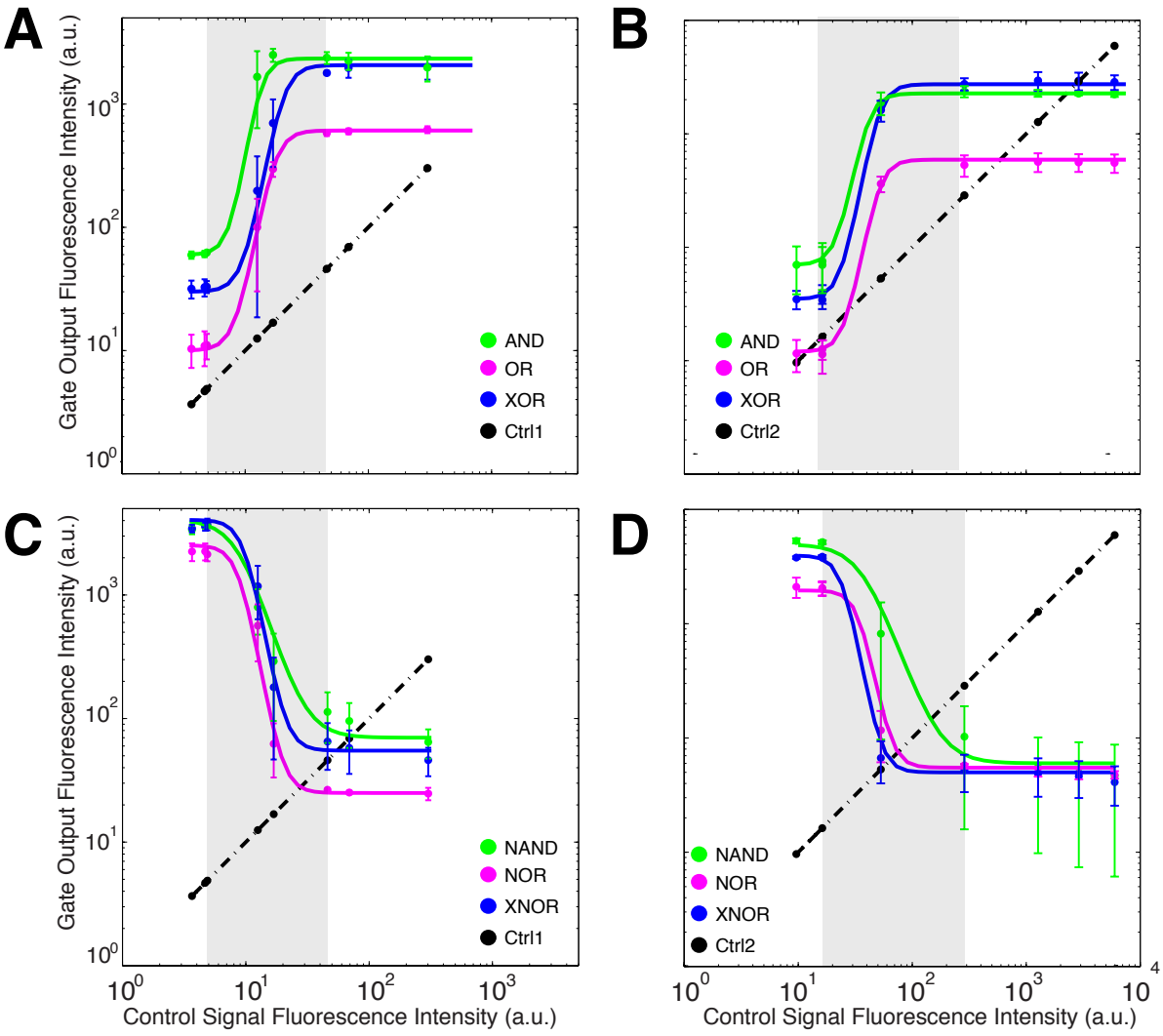

figure S10: Population average, raw GFP values for gate outputs as a function of GFP levels from control signals. Response of amplifier gates to **(A)** increasing arabinose-mediated expression of TP901-1 integrase and **(B)** increasing aTc-mediated expression of Bxb1 integrase. The raw Green Fluorescent Protein (GFP) intensity produced by the gates (colored lines, as noted) is plotted against the raw GFP intensity driven by the integrase expression controllers (dashed straight line). The common switching range is highlighted by the gray box. Response of inverting amplifier gates: **(C)** as in (A), and **(D)** as in (B).

fig. S11

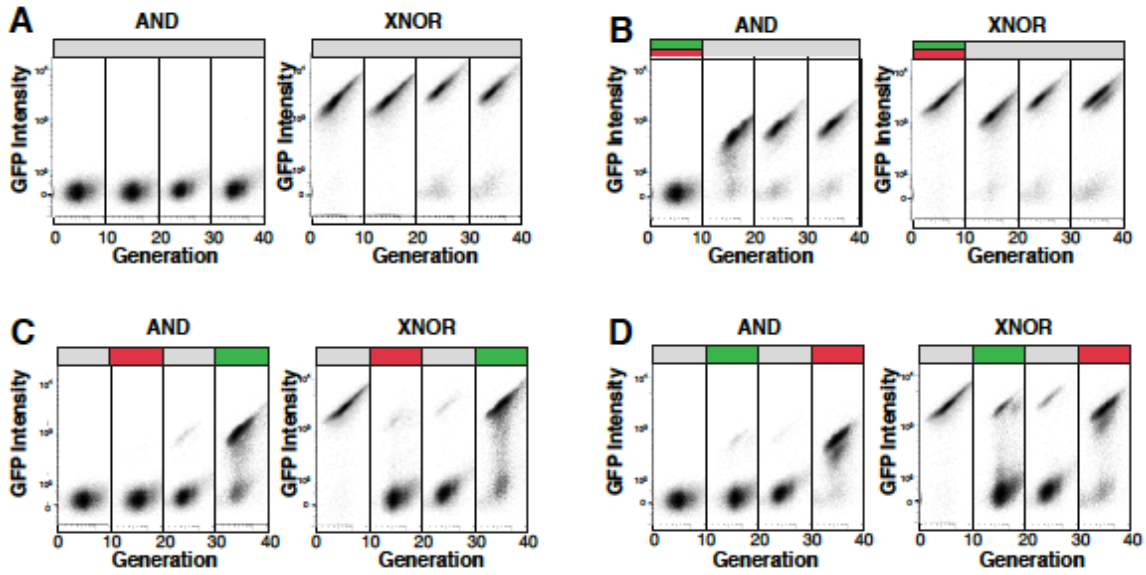

figure S11: Sequential input logic and multi-generation logic registers. (A) Cells containing AND or XNOR logic gates grown for 40 generations with no control signals. Single cell gate output distributions were observed every 10 generations via flow cytometry (forward scatter, x-axis; GFP intensity, y-axis). **(B)** Cells as before exposed to a pulse of both arabinose (red bar) and aTc (green bar) control signals immediately after culture inoculation followed by no further control signals. **(C)** Cells as before exposed to time-separated pulses control inputs starting at generation 10. **(D)** As in (C) but with the relative timing of control inputs reversed.

fig. S12

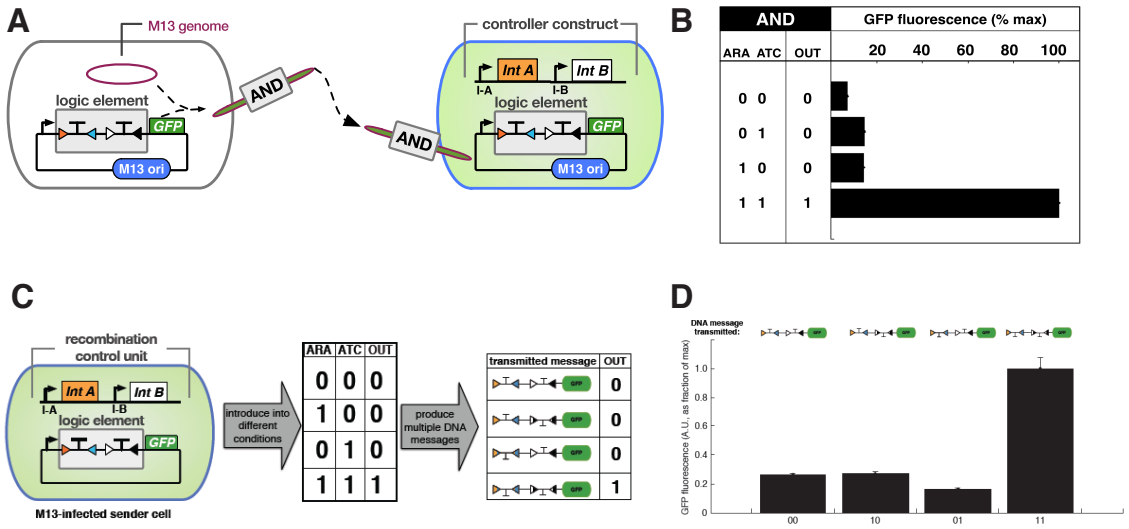

figure S12: Cell-cell communication of programmable DNA logic. (A) Sender cells encoding a Boolean integrase AND gate within a bacteriophage M13 messaging phagemid were co-cultured with receiver cells encoding a recombination control element under the control of exogenous arabinose and aTc induction. Sender cells package the AND gate within M13 phage particles that are secreted into the media and transfect receiver cells. **(B)** AND gate performance within receiver cells. Bulk fluorescence was measurement by platereader (triplicate experiments). **(C)** Sender cells encoding a Boolean integrase AND gate within a bacteriophage M13 messaging phagemid were transformed with the recombination control element and exposed to different combination of arabinose and aTc to generate the four possible states of the AND gate. **(D)** Conservation of DNA states during DNA messaging. Bulk fluorescence from receiver cells co-cultured with senders containing AND gate in different intermediate states was measured by plate-reader (triplicate experiments). All co-cultures were incubated for 5 hours without antibiotic selection followed by 16 hours of outgrowth under conditions selecting for message transmission.

fig. S13

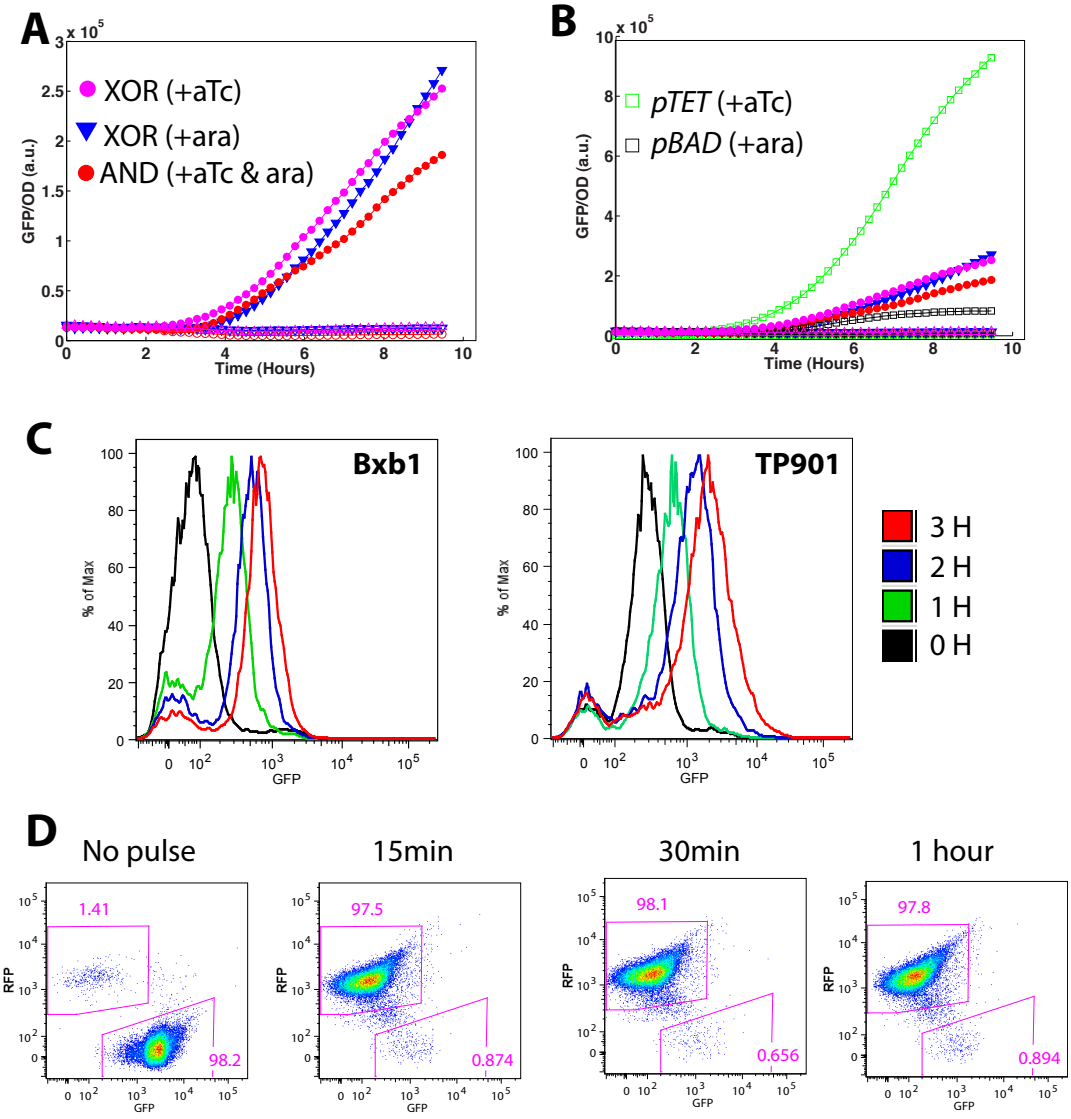

figure S13: **Kinetic measurement of gates operation and individual recombinases properties. (A)** Plate reader measurement of XOR and AND gate induction kinetics, as indicated. Curves of the same color with open symbol are the same samples but uninduced. An increase in output fluorescence is detectable starting between 3 and 4 hours. **(B)** As in (A) but with control signal promoters plotted on the same graph (squares). Note that control signals were induced with max. concentration of inducers. **(C)** Flow cytometry measurements of recombination kinetics of Bxb1 and TP901 both under the control of the pBAD promoter *((5),* plasmid map *J,* respectively*)* using a target plasmid expressing GFP upon DNA inversion (plasmid maps L and M). After 1 hour, an homogenous increase in the cell population fluorescence is detectable. **(D)** Minimal input time assays for pBAD-Bxb1-Set-Generator (*5)*. Cells were incubated with arabinose for the indicated time, washed, diluted 1:1000 and grown overnight before being assayed by flow cytometry. A 15 min. inducer pulse is sufficient to flip more than 95% of the cell population. See also Supplementary Movie 1.

fig S14

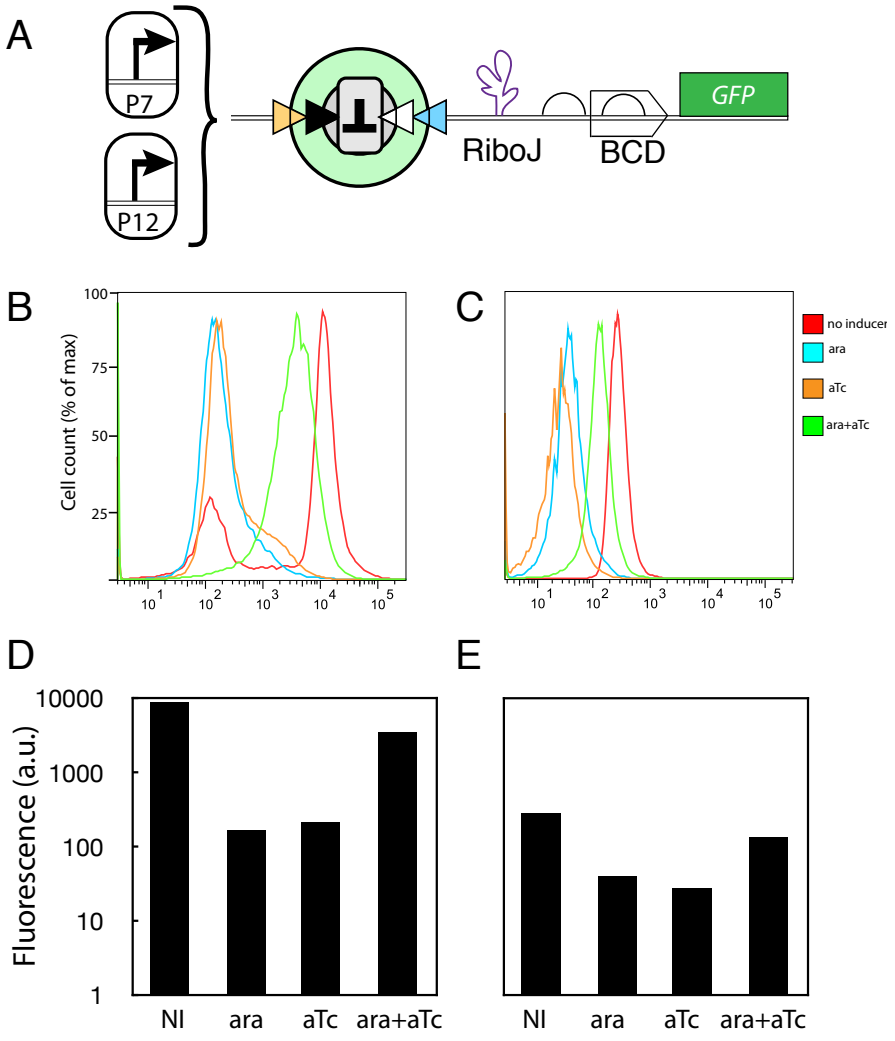

figure S14: Gate output can be tuned by only changing the input promoter. (A) A XNOR gate version using a RiboJ-BCD 5'UTR was used *(24, 44)*. 2 promoters from the BIOFAB collection were used as input signal: P7 and P12, in which P12 is ~6 times weaker than P7 *(44)*. **(B), (C)** Cells containing the dual-controller plasmid and the P7-XNOR (B) or P12-XNOR (C) were grown in different inducers combinations in azure media for 16 hours at 37 C (aTc: 200ng/ml, ara: 0.1% w/v). **(D), (E)** Comparison of whole population median fluorescence intensity between P7-XNOR (D) and P12-XNOR (E).

fig. S15

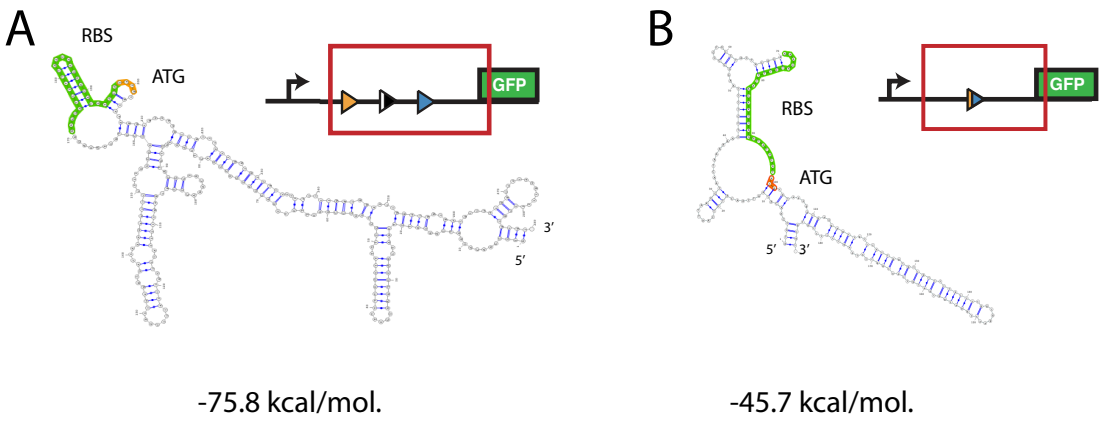

figure S15: Example of predicted structural differences in mRNA encoded by the Boolean integrase logic gates in different states. (A) The OR gate 5'UTR after Bxb1 mediated terminator excision. **(B)** The OR gate 5'UTR after TP901 mediated terminator excision. The RBS is highlighted in green and the start codon in orange. Note the difference in free energy between the two predicted mRNA folds due to a different 5'UTR region. Difference in 5'UTR regions are well known to influence downstream CDS expression through changes in mRNA stability and/or in translation initiation efficiencies. Such isssues have recently been addressed by different groups (*24, 27*), and could likely be reapplied to engineer a second generation of Boolean integrase logic gates. The RNA structure models include the gate sequences plus the first 90 nucleotides of the GFP coding sequence. Structures were calculated using the rnafold software (http://rna.tbi.univie.ac.at/cgi-bin/RNAfold.cgi) using the free energy minimization algorithm and built using the Varna applet (http://varna.lri.fr).

fig. S16

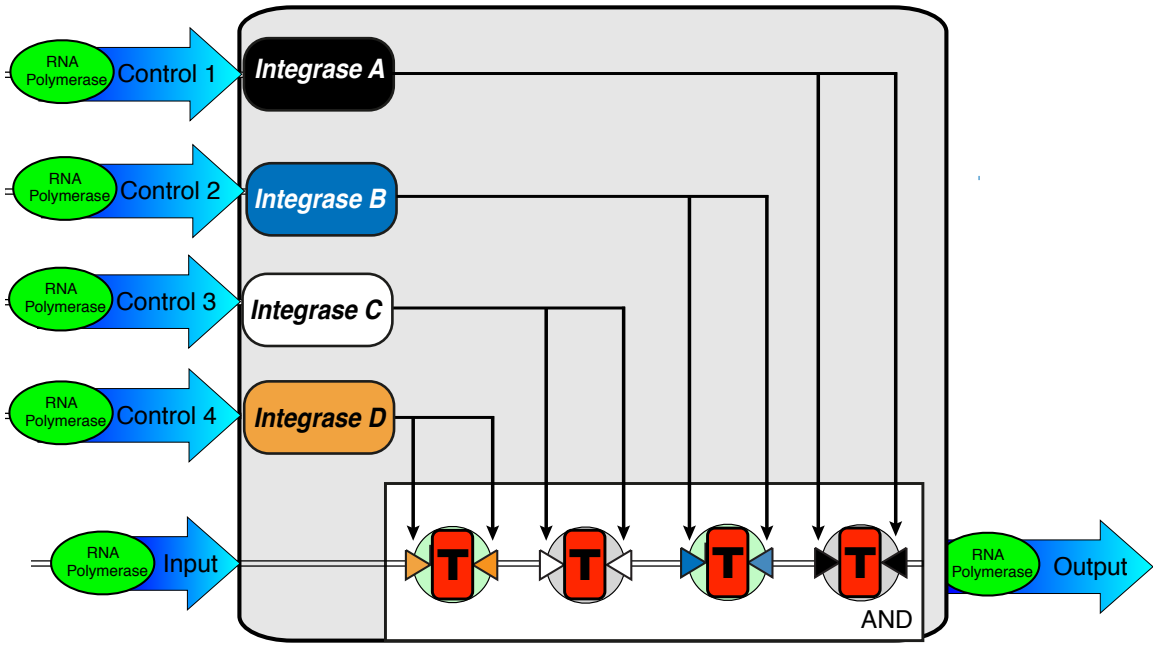

figure S16: Design for a four control signal Boolean integrase AND gate. Four independent integrases control the inversion of four asymmetric terminators serially positioned along the DNA strand. All four terminators must be inverted to obtain a high output from the gate.

<u>Appendix 1</u>: Numerical values and standard deviations (SD) of OD600 for the plate reader measurements used to develop the experimental dual control plots presented in Main Text Figure 2.

AND_OD_avg =

0.2952	0.29313	0.2444	0.26617	0.24544	0.2527
0.32112	0.26721	0.26721	0.28483	0.25995	0.25166
0.2444	0.25684	0.28172	0.28691	0.2838	0.27343
0.30453	0.28898	0.30868	0.31179	0.29313	0.30557
0.28276	0.27758	0.28794	0.30142	0.29416	0.25477
0.3149	0.28691	0.29313	0.29935	0.31697	0.31801

AND_OD_SD =

0.011213	0.070668	0.058542	0.057036	0.032469	0.028897
0.052441	0.078122	0.050051	0.058871	0.0089778	0.01616
0.08643	0.085303	0.099196	0.062921	0.056095	0.057598
0.047878	0.035048	0.037492	0.057794	0.037492	0.070531
0.063126	0.058871	0.022498	0.029668	0.031461	0.045813
0.0762	0.028219	0.064515	0.017129	0.032469	0.08088

OR_OD_avg =

0.24337	0.27654	0.25166	0.28483	0.22989	0.21641
0.27239	0.30971	0.27965	0.26514	0.31075	0.27965
0.26825	0.3066	0.27965	0.26617	0.31801	0.24959
0.30246	0.30453	0.32215	0.29416	0.34911	0.28691
0.24544	0.26514	0.27654	0.27965	0.25892	0.22263
0.22678	0.28276	0.28587	0.27136	0.28069	0.26721

OR_OD_SD =

0.062304	0.052318	0.05909	0.048414	0.035323	0.027172
0.073486	0.031152	0.027642	0.033254	0.09392	0.082927
0.070942	0.043577	0.04828	0.027172	0.068796	0.032667
0.057036	0.038968	0.014364	0.012569	0.027875	0.042339
0.06842	0.025138	0.037835	0.037707	0.028729	0.059525
0.04937	0.035048	0.026572	0.010922	0.023549	0.035866

XOR_OD_avg =

0.32112	0.30246	0.32112	0.31801	0.29416	0.26306
0.28794	0.2952	0.31075	0.29624	0.29727	0.29105
0.34703	0.33667	0.33356	0.32837	0.32215	0.28898
0.3066	0.33045	0.33874	0.3377	0.32215	0.29624
0.30764	0.29209	0.31593	0.28898	0.29105	0.2838

```
      0.30764      0.31904      0.32112       0.3066      0.30142      0.30971


XOR_OD_SD =

     0.072091      0.07162     0.025329     0.052257     0.031152     0.014024
     0.032667     0.057598     0.051761     0.015959     0.049598     0.065997
     0.053627     0.038636    0.0089778     0.023549     0.012948     0.029992
     0.028219     0.021844     0.020394     0.020707     0.027172     0.026082
       0.0311     0.026572     0.018223     0.011213     0.014024     0.027172
     0.036666     0.021844     0.029559     0.047608     0.045175     0.012948


NAND_OD_avg =

      0.22678      0.21434      0.23767        0.233      0.22367      0.21279
      0.21434      0.22056      0.24855        0.247      0.28121        0.247
      0.21745      0.21901      0.23766      0.25633      0.26099      0.23145
      0.19723      0.21279      0.24855      0.26254      0.23456      0.29053
       0.2159      0.20967      0.22523      0.25321      0.25477      0.24389
        0.247      0.22989      0.25477      0.26255      0.25788      0.22989


NAND_OD_SD =

     0.017593    0.0087964      0.02419     0.021991     0.026389      0.02419
     0.035186    0.0043982    0.0087964     0.019792     0.032987     0.019792
     0.057177     0.010996    0.0021991     0.032987     0.026389     0.010996
     0.063774     0.028588    0.0043982     0.019792     0.010996     0.059376
     0.050579     0.050579     0.050579    0.0021991     0.026389     0.041783
      0.07257      0.04838      0.04838    0.0065973    0.0043982    0.0043982


NOR_OD_avg =

      0.32008      0.28794      0.29313      0.30868      0.27239      0.23507
      0.30038      0.31179      0.32734      0.32112      0.28587      0.29002
      0.32112       0.3066      0.31179      0.27654      0.27447      0.30971
      0.30453      0.30038      0.31179      0.28794      0.28794      0.29313
      0.29831      0.28172      0.26721      0.24959       0.2641      0.24855
      0.32423       0.3149      0.27758       0.2838      0.29935       0.2838


NOR_OD_SD =

     0.035323     0.034956     0.036046     0.068231     0.028729     0.025138
     0.045318     0.090796      0.08283     0.079432     0.070646     0.074662
     0.041995     0.051323     0.054343      0.02348     0.033544     0.074662
     0.042755       0.0529     0.042906    0.0095012     0.025329       0.0472
     0.032469     0.038636     0.017316     0.011774     0.044092     0.041141
     0.042906     0.045848     0.017129     0.017129     0.038005     0.069981
```

```
XNOR_OD_avg =

      0.34185      0.32786      0.29831      0.33563      0.21279      0.23611
      0.31231      0.31853      0.31231      0.31853      0.28587      0.25477
       0.3263      0.35274       0.3403      0.33719      0.27499      0.26099
      0.31697      0.31075      0.33252      0.33408      0.32008      0.29675
      0.28743      0.30142      0.33874      0.33874      0.31697      0.26876
      0.32786      0.32475      0.33874       0.3403      0.31853      0.29831


XNOR_OD_SD =

     0.013195     0.015394     0.013195     0.070371     0.054978    0.0043982
    0.0065973     0.010996    0.0021991    0.0065973     0.026389     0.013195
     0.017593     0.041783      0.07257     0.032987     0.015394    0.0087964
     0.017593     0.013195     0.026389      0.02419      0.04838     0.010996
     0.015394     0.021991     0.021991            0    0.0043982     0.028588
     0.028588    0.0065973    0.0043982     0.010996     0.041783     0.026389
```

<u>Appendix 2</u>: Numerical values and standard deviations (SD) of GFP intensity for the plate reader measurements used to develop the experimental dual control plots presented in Main Text Figure 2.

AND (GFP/OD) =

6621.1	8575.9	1.0367e+05	1.0927e+05	1.0937e+05	1.0294e+05
4078.9	18631	71900	97169	80649	79889
3479.4	8456.5	28417	35453	34520	40759
2111.9	2263.7	3546.1	5005.6	6666.5	8689
2221.4	2738.1	3374.8	4660.8	5010.3	6291.7
1969.2	2048.8	3026.1	3799.8	5160.3	5874.4

AND_SD =

2688	1600.5	8525.9	8184.9	17931	8309.5
1179.6	21720	19069	11112	6196.5	5488.7
1171.4	10385	38506	29545	40672	42772
263.85	530.17	979.56	1501.2	3854.8	5920.1
841.87	922.36	1165	653.36	2349.6	1634.8
854.91	897.99	1180.5	940.3	1705.8	1332.4

OR (GFP/OD) =

39938	47332	64088	83729	1.1154e+05	1.1312e+05
33099	36746	52548	77566	85242	98759
8435.8	9451.9	26018	59341	66276	91239
2673.4	4148.6	17917	47868	66654	85734
3148.5	5276.5	21179	54346	79187	1.0449e+05
2920.7	3850.1	14412	54534	79039	85024

OR_ SD =

4873.6	13239	14718	12554	21445	21805
7304.2	10000	9260	16367	13526	26485
9554.4	10515	20228	23393	13834	24729
483.65	2225.6	10600	12353	18921	22619
739.05	2641.1	23702	19340	23030	36954
1182.6	1486.5	8108.8	10712	32239	21952

XOR (GFP/OD) =

97466	1.0226e+05	52447	15657	13593	10328
75920	77761	70149	27781	21113	16108
7954.6	5352.8	17672	70960	80904	72932
4147.9	4663.9	16668	77085	89253	85172
4505	5787.3	15807	85069	97891	1.0085e+05
4037.6	5327.6	12599	81244	96891	92228

XOR_ SD =

35049	44059	21845	6323.7	5868.3	3617
36867	39567	22730	9760.7	9445.3	6278.6
5233.9	1277	1736	20814	29706	18116
1387.2	1036.8	4438.2	9494.6	21447	7486.7
648.29	1452.6	7253.8	11676	27915	15739
254.85	854.22	3828.4	11282	20726	13049

NAND(GFP/OD) =

3.3622e+05	3.5218e+05	2.1329e+05	99729	77936	76817
3.3431e+05	3.8059e+05	2.574e+05	1.542e+05	84090	78804
5.8208e+05	6.6315e+05	4.9814e+05	3.9412e+05	3.6318e+05	3.5761e+05
7.0418e+05	7.3472e+05	6.4686e+05	6.1739e+05	7.4259e+05	5.9855e+05
6.7389e+05	7.3897e+05	6.1321e+05	5.4242e+05	5.6473e+05	5.4577e+05
6.3287e+05	7.1337e+05	5.8596e+05	5.8903e+05	6.2565e+05	6.3932e+05

NAND_ SD =

58801	40712	1.1441e+05	39770	36329	39146
86648	1.3163e+05	91815	76721	40564	46346
1.5715e+05	1.4243e+05	1.9812e+05	1.4619e+05	2.5546e+05	2.3957e+05
11368	97694	89480	21825	97664	79543
3273.4	18821	5406	4501.8	14415	13101
58803	31336	29521	98789	65661	1.1022e+05

NOR (GFP/OD) =

18883	19054	11205	3658.5	3529.3	4716.2
32665	48612	15497	4784.6	3928.2	3658
1.0911e+05	1.0393e+05	76423	15116	8233.9	6713.4
1.6275e+05	1.4517e+05	87396	13267	8495.8	6864.7
1.6248e+05	1.438e+05	87920	13810	9034.6	6665.9
1.5628e+05	1.6229e+05	89103	15830	8766.5	6246.7

NOR_ SD =

4311.6	4422.1	4066.9	1182.8	158.34	547.51
12313	45431	8761.2	1977.9	1662.2	557.77
64785	34878	48756	11804	5249.6	1110.4
13802	17338	42360	9421.4	3580.9	690.96
10277	29142	55526	9707.1	4266.7	1000.3
16376	9311	61068	11941	2942.6	1025.6

XNOR (GFP/OD) =

86907	1.068e+05	3.8816e+05	6.8936e+05	6.9736e+05	5.9656e+05
85863	1.2738e+05	4.1851e+05	5.5173e+05	5.8615e+05	5.2688e+05
2.004e+05	2.8565e+05	2.8234e+05	3.0046e+05	4.4083e+05	3.0108e+05
5.577e+05	5.877e+05	1.0098e+05	25070	24521	18461
6.3308e+05	7.2948e+05	1.0264e+05	28348	23541	19690

```
   6.1967e+05   5.8398e+05   1.3152e+05        22111        20845        17337


XNOR_ SD =

       5991.7        16845   1.7166e+05        66185   1.7336e+05        18301
       1931.9       7204.5   1.9091e+05        99003         6245        21524
        83127   1.6112e+05       5505.6        57425        63250   1.4369e+05
   1.3611e+05   1.0429e+05        26607        12750       1746.5       9115.8
   1.6676e+05        62539        62778       7720.9       2331.4       6337.6
    1.923e+05   1.8354e+05        29286        12972       8343.6       9764.8
```

Appendix 3: Plasmids Maps

(**A**) The dual controller plasmid with pBad-TP901 and pTET-Bxb1. (**B**) The measurement plasmid where the Bxb1 integrase is replaced by the superfolder-GFP cassette (**C**) The measurement plasmid where the TP901 integrase is replaced by the superfolder-GFP cassette. **(D)** to **(I)** the different logic gates plasmids. **(J)** the pBAD-TP901-Set-Generator **(K)** The TP901 BP register with RFP and GFP outputs. **(L)** and **(M)** the Bxb1 and TP901 BP register expressing GFP upon flipping.

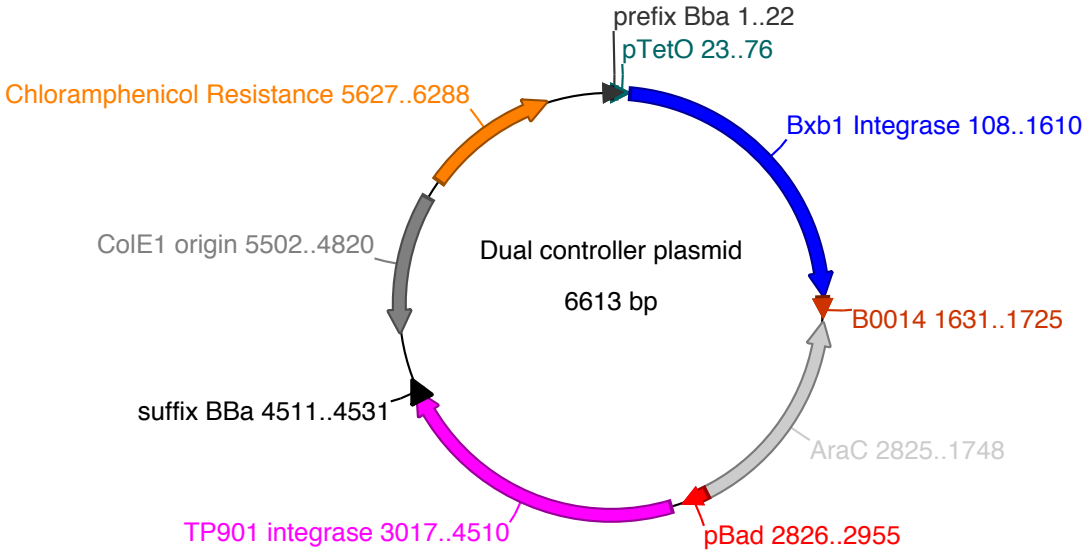

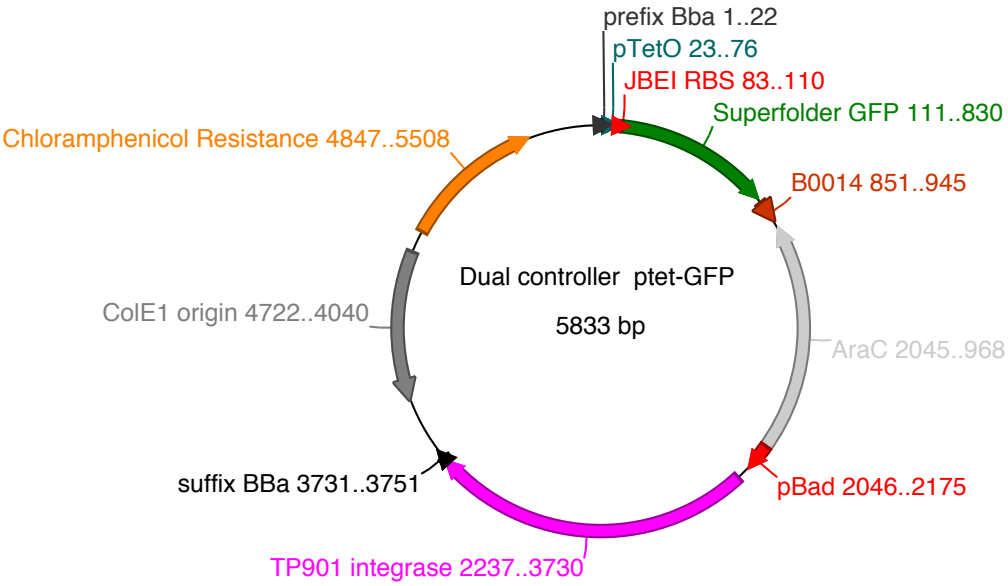

A

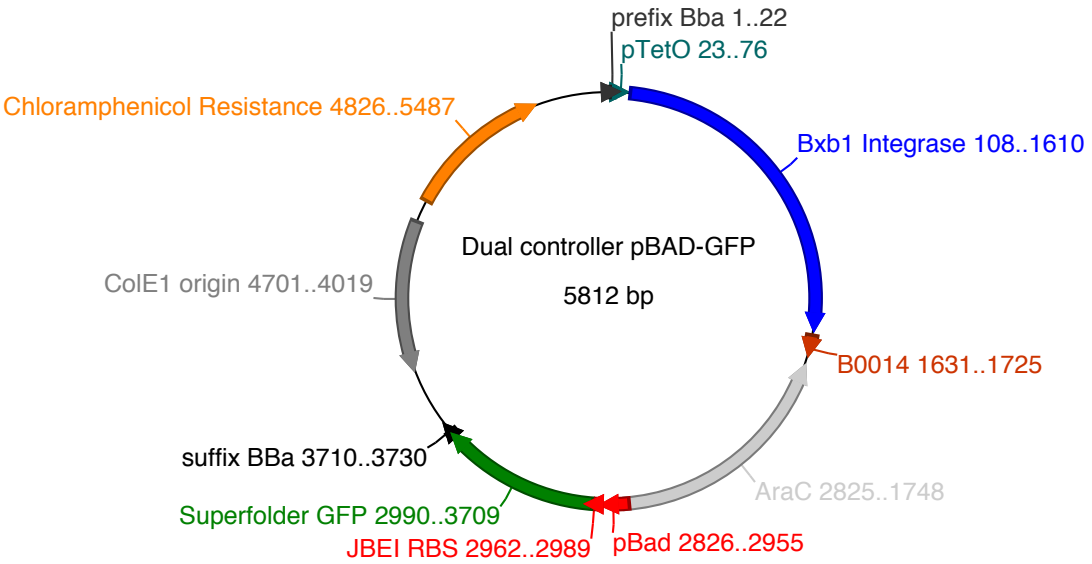
prefix Bba 1..22
pTetO 23..76
Chloramphenicol Resistance 4826..5487
Bxb1 Integrase 108..1610
Dual controller pBAD-GFP
5812 bp
ColE1 origin 4701..4019
B0014 1631..1725
suffix BBa 3710..3730
AraC 2825..1748
Superfolder GFP 2990..3709
JBEI RBS 2962..2989
pBad 2826..2955

B

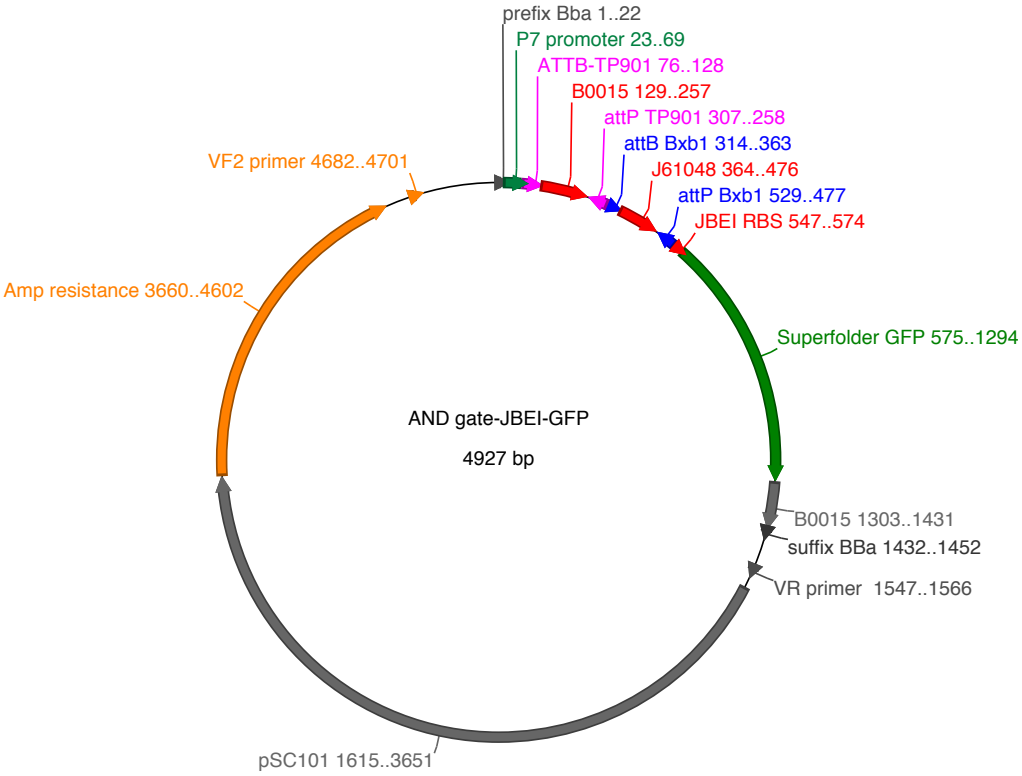
prefix Bba 1..22
P7 promoter 23..69
ATTB-TP901 76..128
B0015 129..257
attP TP901 307..258
attB Bxb1 314..363
J61048 364..476
attP Bxb1 529..477
JBEI RBS 547..574
VF2 primer 4682..4701
Amp resistance 3660..4602
Superfolder GFP 575..1294
AND gate-JBEI-GFP
4927 bp
B0015 1303..1431
suffix BBa 1432..1452
VR primer 1547..1566
pSC101 1615..3651

C

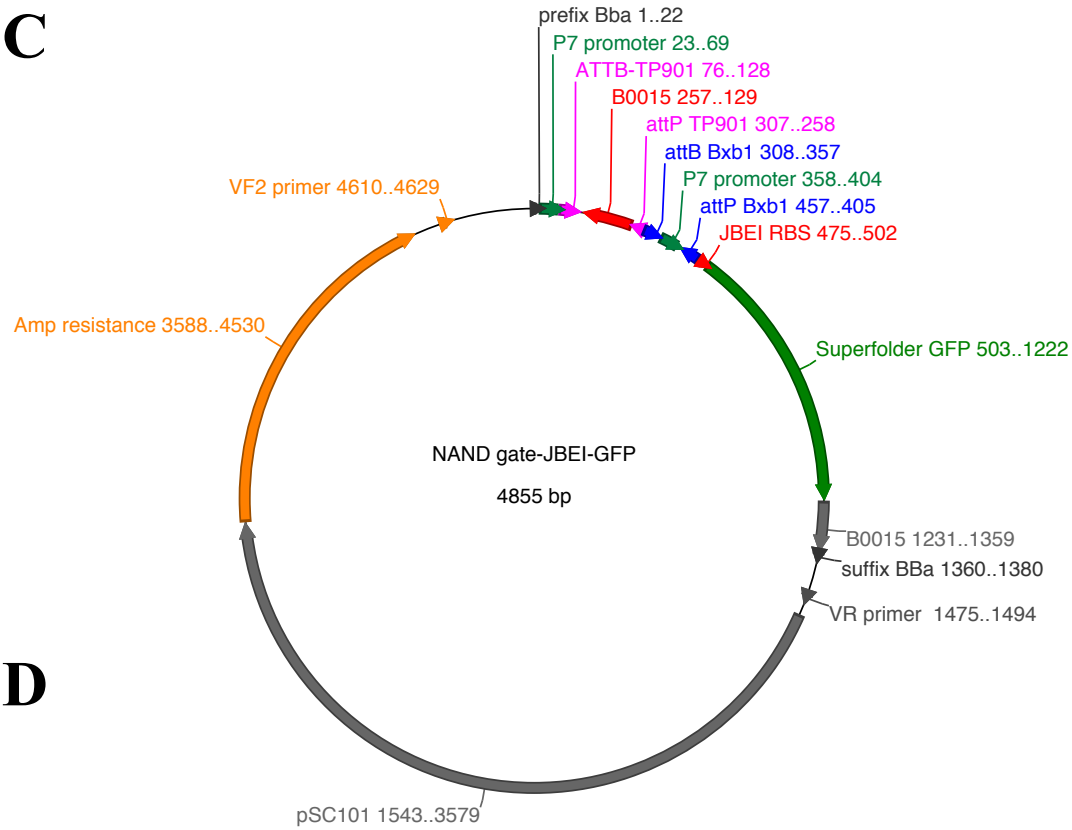
prefix Bba 1..22
P7 promoter 23..69
ATTB-TP901 76..128
B0015 257..129
attP TP901 307..258
attB Bxb1 308..357
P7 promoter 358..404
attP Bxb1 457..405
JBEI RBS 475..502
VF2 primer 4610..4629
Amp resistance 3588..4530
Superfolder GFP 503..1222
NAND gate-JBEI-GFP
4855 bp
B0015 1231..1359
suffix BBa 1360..1380
VR primer 1475..1494
pSC101 1543..3579

D

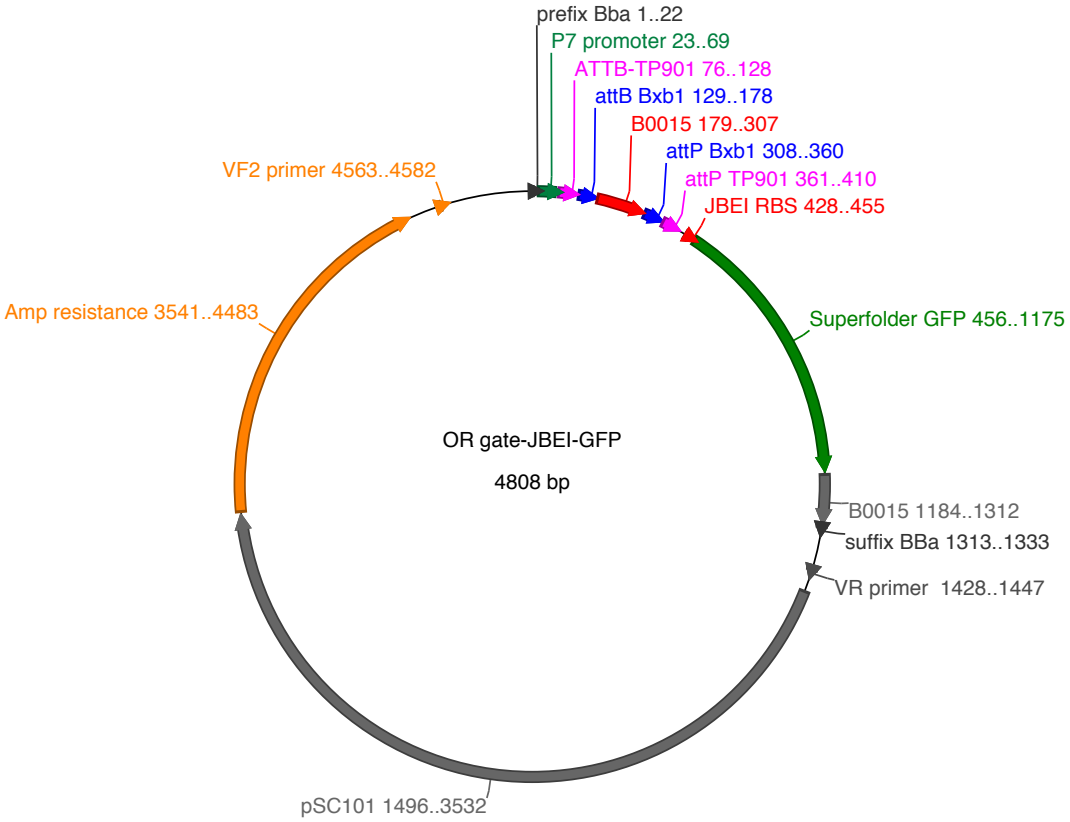
prefix Bba 1..22
P7 promoter 23..69
ATTB-TP901 76..128
attB Bxb1 129..178
B0015 179..307
attP Bxb1 308..360
attP TP901 361..410
JBEI RBS 428..455
VF2 primer 4563..4582
Amp resistance 3541..4483
Superfolder GFP 456..1175
OR gate-JBEI-GFP
4808 bp
B0015 1184..1312
suffix BBa 1313..1333
VR primer 1428..1447
pSC101 1496..3532

E

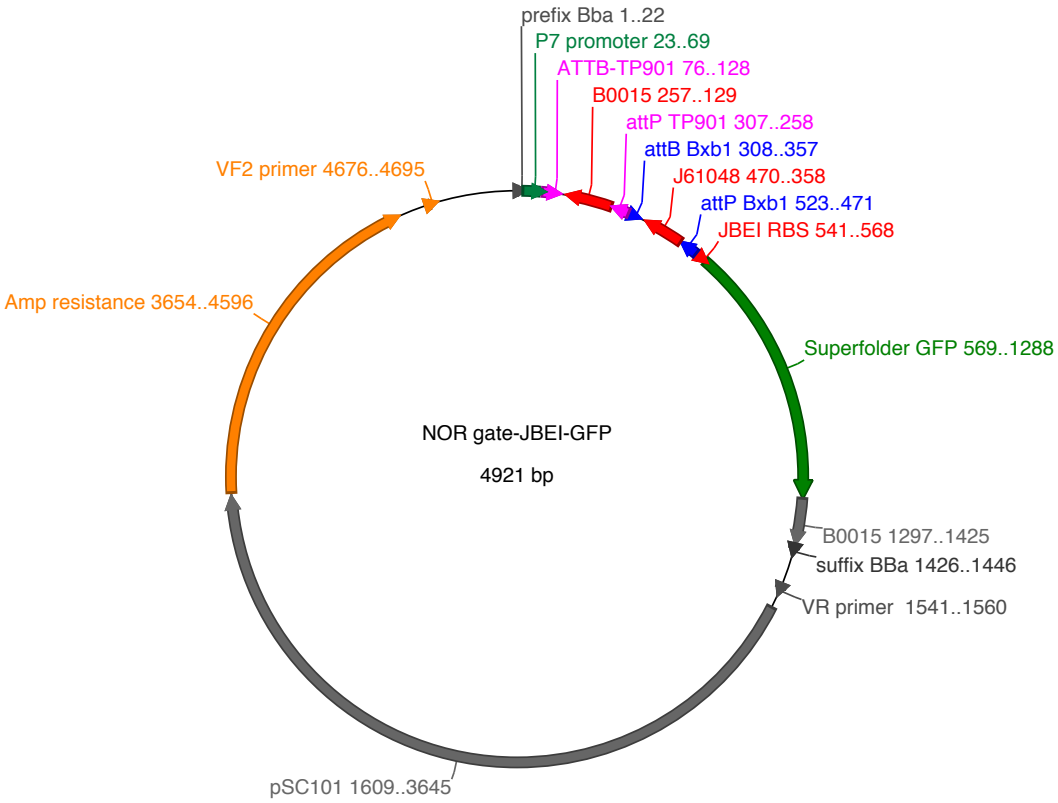
prefix Bba 1..22
P7 promoter 23..69
ATTB-TP901 76..128
B0015 257..129
attP TP901 307..258
attB Bxb1 308..357
J61048 470..358
attP Bxb1 523..471
JBEI RBS 541..568
VF2 primer 4676..4695
Amp resistance 3654..4596
Superfolder GFP 569..1288
NOR gate-JBEI-GFP
4921 bp
B0015 1297..1425
suffix BBa 1426..1446
VR primer 1541..1560
pSC101 1609..3645

F

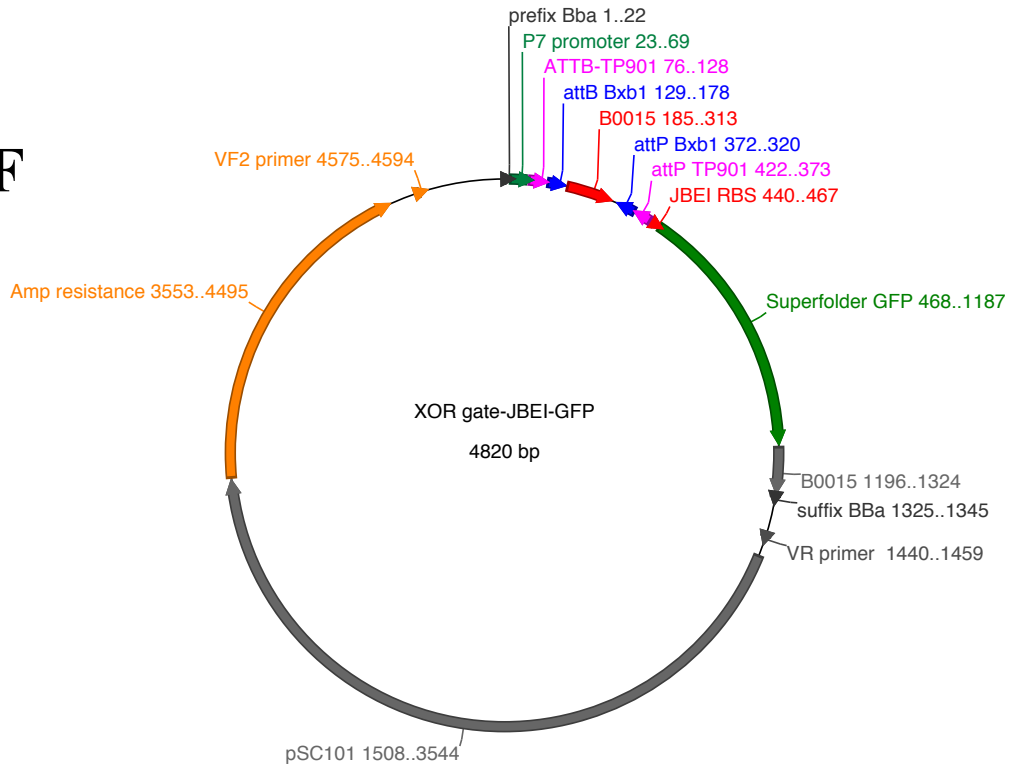
prefix Bba 1..22
P7 promoter 23..69
ATTB-TP901 76..128
attB Bxb1 129..178
B0015 185..313
attP Bxb1 372..320
attP TP901 422..373
JBEI RBS 440..467
VF2 primer 4575..4594
Amp resistance 3553..4495
Superfolder GFP 468..1187
XOR gate-JBEI-GFP
4820 bp
B0015 1196..1324
suffix BBa 1325..1345
VR primer 1440..1459
pSC101 1508..3544

G

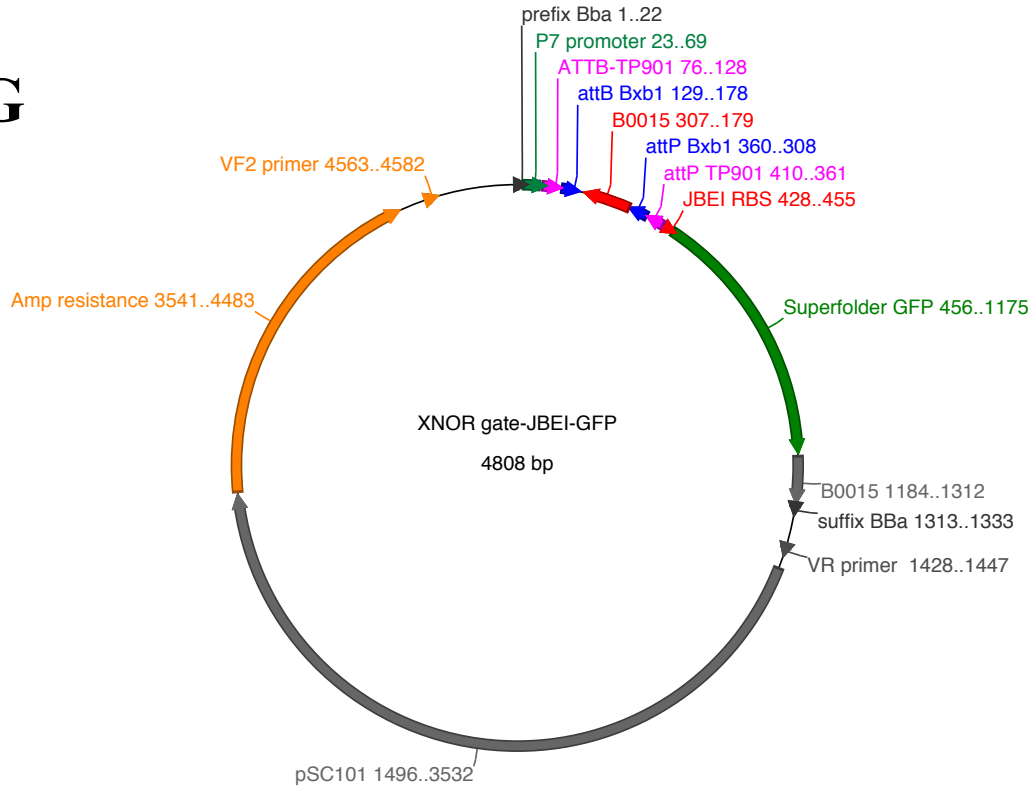
prefix Bba 1..22
P7 promoter 23..69
ATTB-TP901 76..128
attB Bxb1 129..178
B0015 307..179
attP Bxb1 360..308
attP TP901 410..361
JBEI RBS 428..455
VF2 primer 4563..4582
Amp resistance 3541..4483
Superfolder GFP 456..1175
XNOR gate-JBEI-GFP
4808 bp
B0015 1184..1312
suffix BBa 1313..1333
VR primer 1428..1447
pSC101 1496..3532

H

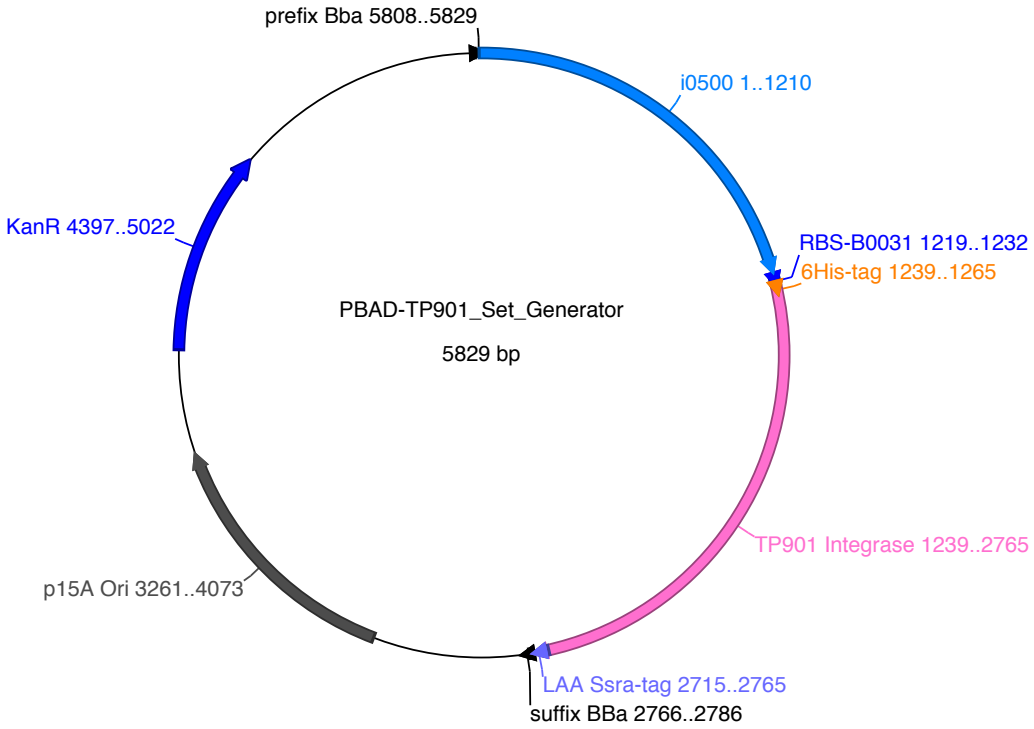
prefix Bba 5808..5829
i0500 1..1210
KanR 4397..5022
RBS-B0031 1219..1232
6His-tag 1239..1265
PBAD-TP901_Set_Generator
5829 bp
TP901 Integrase 1239..2765
p15A Ori 3261..4073
LAA Ssra-tag 2715..2765
suffix BBa 2766..2786

M

I

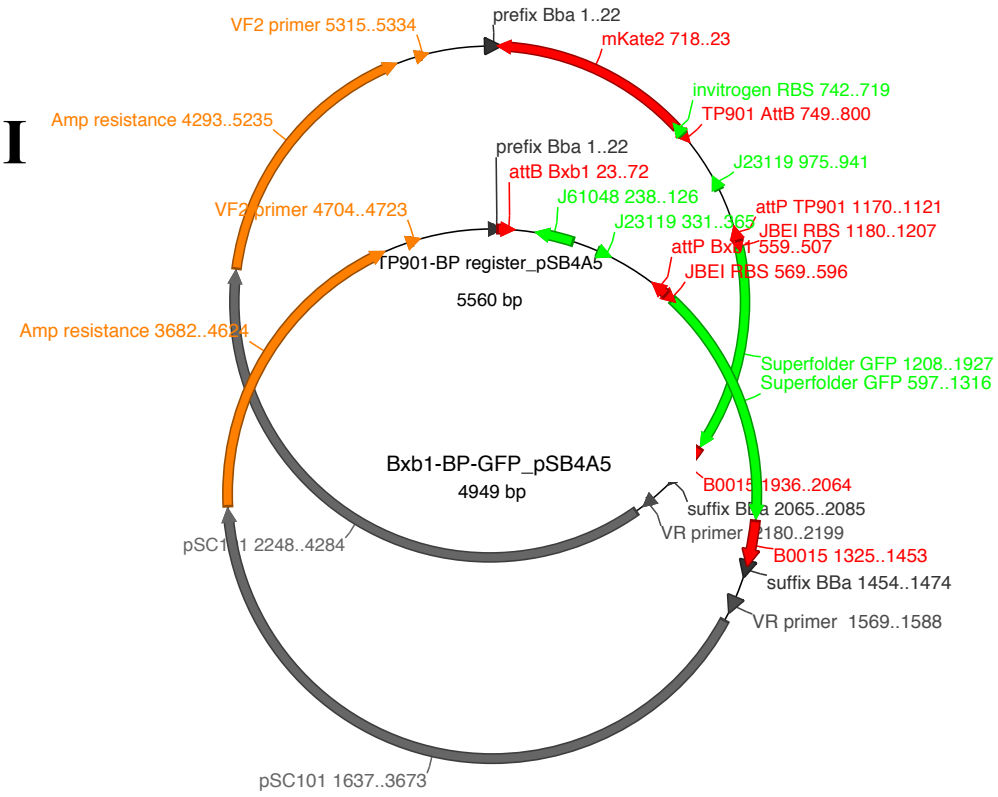
VF2 primer 5315..5334
prefix Bba 1..22
mKate2 718..23
invitrogen RBS 742..719
TP901 AttB 749..800
Amp resistance 4293..5235
prefix Bba 1..22
attB Bxb1 23..72
J23119 975..941
J61048 238..126
attP TP901 1170..1121
VF2 primer 4704..4723
J23119 331..365
JBEI RBS 1180..1207
attP Bxb1 559..507
TP901-BP register_pSB4A5
JBEI RBS 569..596
5560 bp
Amp resistance 3682..4624
Superfolder GFP 1208..1927
Superfolder GFP 597..1316
Bxb1-BP-GFP_pSB4A5
4949 bp
B0015 1936..2064
suffix BBa 2065..2085
VR primer 2180..2199
pSC1 1 2248..4284
B0015 1325..1453
suffix BBa 1454..1474
VR primer 1569..1588
pSC101 1637..3673

J

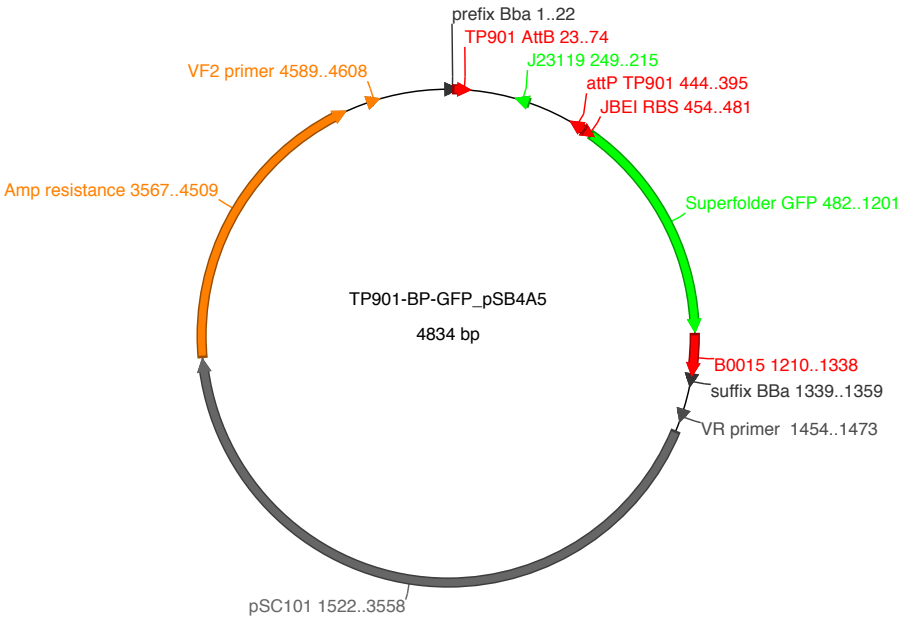
prefix Bba 1..22
TP901 AttB 23..74
J23119 249..215
VF2 primer 4589..4608
attP TP901 444..395
JBEI RBS 454..481
Amp resistance 3567..4509
Superfolder GFP 482..1201
TP901-BP-GFP_pSB4A5
4834 bp
B0015 1210..1338
suffix BBa 1339..1359
VR primer 1454..1473
pSC101 1522..3558

Appendix 4: Sequences of primers used in this study.

G1004	gtttcttcgaattcgcggccgcttctag
JB-422	acattgattatttgcacggcgtcac
JB-423	CTGCAGCGGCCGCTACTAGTATTAAGCAGCCAGAGCGTAGTTTTCG
JB-424	gctaatcttatggataaaaatgctatggcatagc
JB-425	CGAAAACTACGCTCTGGCTGCTTAATACTAGTAGCGGCCGCTGCAG
JB-431	aAAGCAAATAAATTTTTTctctagaagcggccgcgaattc
JB-434	GCCtacTAGAGAAAAGATCTTTTAAGAAGGAGATATACAT
JB-435	ATGTATATCTCCTTCTTAAAAGATCTTTTCTCTAgtaGGCGCGCCgcgagtttttatttc
JB-457	TAACATCTCAATCAAGGTAAATGCTTTTTGCT
JB-458	ATGTATATCTCCTTCTTAAAAGATCTTTTCCTAGTAGG
JB-459	GGCGCGCCTACTAGGAAAAG
JB-460	GCAAAAAAAGCAAAAAGCATTTACCTTGATTG
JB-466	TAACATCTCAATCAAGGTAAATGCTTTTTGCTTTTTTTTGC
JB-468	GCAAAAAAAGCAAAAAGCATTTACCTTGATTGAGATGTTA
JB-469	TGAGACCGCGGTGGTTGACC
JB-470	TACTAGAGAAAAGATCTTTTAAGAAGGAGATATACATATGCG
JB-471	CATATGTATATCTCCTTCTTAAAAGATCTTTTCTctagtaTCGTGGTTTGTCTGGTCAACC
JB-472	CATATGTATATCTCCTTCTTAAAAGATCTTTTCTctagtagcgagttttatttcgtttatttcaattaaggtaac
JB-473	CATATGTATATCTCCTTCTTAAAAGATCTTTTCTctagtaaaaggagtttttagttaccttaattgaaataaacgaaataaaa
JB-483	ctagtaTCGTGGTTTGTCTGGTCAACCACCGCGGTCTCAGTGGTGTACGGTACAAACCCcgg
JB-508	AGAGATACTGAGCACAAGCTTAAAGATCTTTTAAGAAGGAGATATACATatgcgtaaagg
JB-509	gtgaTTATTAATGCATgcggccgctcatcatttgtacagttcatccataccatg
JB-510	CTCCTTCTTAAAAGATCTTTAAGCTTGTGCTCAGTATCTCTATCACTG
JB-511	actgtacaaatgatgagcggccgcATGCATTAATAAtcac
JB-512	ttttttgggctagcTACTAGAAAGATCTTTTAAGAAGGAGATATACATatgcgtaaagg
JB-513	CTGCAGCGGCCGCTACTAGTAtcatcatttgtacagttcatccataccatgc
JB-514	gcatATGTATATCTCCTTCTTAAAAGATCTTTCTAGTAgctagcccaaaaaaacggtatg
JB-515	tgaactgtacaaatgatgaTACTAGTAGCGGCCGCTGCAG
JB-518	GGCATGCCTCGAGATGCATG
JB-519	AGGATCCCCGGGTACCGAGC
JB-520	TTGGGGATCGGAATTCGAGCTCGGTACCCGGGGATCCTgaattcgcggccgcttctagag
JB-521	TCAGTTTAGGTTAGGCGCCATGCATCTCGAGGCATGCCctgcagcggccgctactagta
JB-549	ccattcgccattcaggctgcgcaactgttgggaagggcgaattcgcggccgcttctagag
JB-550	gagtgagctgataccgctcgccgcagccgaacgaccgagctgcagcggccgctactagta
JB-551	cgctacagggcgcgtc
JB-552	ccctgattctgtggataaccgt

References and Notes

1. B. Wang, M. Buck, Customizing cell signaling using engineered genetic logic circuits. *Trends Microbiol.* **20**, 376 (2012). doi:10.1016/j.tim.2012.05.001 Medline

2. Y. Benenson, Biomolecular computing systems: principles, progress and potential. *Nat. Rev. Genet.* **13**, 455 (2012). doi:10.1038/nrg3197 Medline

3. T. Miyamoto, S. Razavi, R. DeRose, T. Inoue, Synthesizing biomolecule-based Boolean logic gates. *ACS Synth. Biol.* **2**, 72 (2012). doi:10.1021/sb3001112

4. D. R. Burrill, P. A. Silver, Making cellular memories. *Cell* **140**, 13 (2010). doi:10.1016/j.cell.2009.12.034 Medline

5. J. Bonnet, P. Subsoontorn, D. Endy, Rewritable digital data storage in live cells via engineered control of recombination directionality. *Proc. Natl. Acad. Sci. U.S.A.* **109**, 8884 (2012). doi:10.1073/pnas.1202344109 Medline

6. S. Basu, Y. Gerchman, C. H. Collins, F. H. Arnold, R. Weiss, A synthetic multicellular system for programmed pattern formation. *Nature* **434**, 1130 (2005). doi:10.1038/nature03461 Medline

7. M. E. Ortiz, D. Endy, Engineered cell-cell communication via DNA messaging. *J Biol Eng* **6**, 16 (2012). doi:10.1186/1754-1611-6-16 Medline

8. Y. Y. Chen, M. C. Jensen, C. D. Smolke, Genetic control of mammalian T-cell proliferation with synthetic RNA regulatory systems. *Proc. Natl. Acad. Sci. U.S.A.* **107**, 8531 (2010). doi:10.1073/pnas.1001721107 Medline

9. Z. Xie, L. Wroblewska, L. Prochazka, R. Weiss, Y. Benenson, Multi-input RNAi-based logic circuit for identification of specific cancer cells. *Science* **333**, 1307 (2011). doi:10.1126/science.1205527 Medline

10. A. Tamsir, J. J. Tabor, C. A. Voigt, Robust multicellular computing using genetically encoded NOR gates and chemical ‘wires’. *Nature* **469**, 212 (2011). doi:10.1038/nature09565 Medline

11. T. S. Moon, C. Lou, A. Tamsir, B. C. Stanton, C. A. Voigt, Genetic programs constructed from layered logic gates in single cells. *Nature* **491**, 249 (2012). doi:10.1038/nature11516 Medline

12. S. Ausländer, D. Ausländer, M. Müller, M. Wieland, M. Fussenegger, Programmable single-cell mammalian biocomputers. *Nature* **487**, 123 (2012). Medline

13. For example, converting a NOR gate repressed by transcription factors to an OR gate activated by transcription factors requires changing how proteins interact with RNA polymerase (from competitive binding and occlusion to recruitment and initiation), and simultaneous reworking of the basal activity for core promoter elements (from a constitutively active promoter that can be repressed to a weak promoter that does not spontaneously initiate transcription yet that transcription factors activate).

14. C. Wadey, I. Deese, D. Endy, AiSB Chapter 3, Common Signal Carriers, accessible at *http://hdl.handle.net/1721.1/46337*

15. T. S. Ham, S. K. Lee, J. D. Keasling, A. P. Arkin, Design and construction of a double inversion recombination switch for heritable sequential genetic memory. *PLoS ONE* **3**, e2815 (2008). doi:10.1371/journal.pone.0002815 Medline

16. A. E. Friedland *et al*., Synthetic gene networks that count. *Science* **324**, 1199 (2009). doi:10.1126/science.1172005 Medline

17. P. A. Varadarajan, D. Del Vecchio, Design and characterization of a three-terminal transcriptional device through polymerase per second. *IEEE Trans. Nanobioscience* **8**, 281 (2009). doi:10.1109/TNB.2009.2028687 Medline

18. J. Bardeen, W. Brattain, The transistor, a semi-conductor triode. *Phys. Rev.* **74**, 230 (1948). doi:10.1103/PhysRev.74.230

19. With transistor-based logic, gates use a base, emitter, collector architecture that classically only allows for control of electrical current at one point on a wire by a single signal. Transcriptor-based logic allows RNA polymerase flow at a single point on DNA to be controlled, in theory, by as many independent recombinases as needed.

20. J. A. Lewis, G. F. Hatfull, Control of directionality in integrase-mediated recombination: examination of recombination directionality factors (RDFs) including Xis and Cox proteins. *Nucleic Acids Res.* **29**, 2205 (2001). doi:10.1093/nar/29.11.2205 Medline

21. W. R. A. Brown, N. C. O. Lee, Z. Xu, M. C. M. Smith, Serine recombinases as tools for genome engineering. *Methods* **53**, 372 (2011). doi:10.1016/j.ymeth.2010.12.031 Medline

22. B. Canton, A. Labno, D. Endy, Refinement and standardization of synthetic biological parts and devices. *Nat. Biotechnol.* **26**, 787 (2008). doi:10.1038/nbt1413 Medline

23. Material and methods are available as supporting materials on *Science* Online.

24. C. Lou, B. Stanton, Y.-J. Chen, B. Munsky, C. A. Voigt, Ribozyme-based insulator parts buffer synthetic circuits from genetic context. *Nat. Biotechnol.* **30**, 1137 (2012). doi:10.1038/nbt.2401 Medline

25. L. Pasotti, N. Politi, S. Zucca, M. G. Cusella De Angelis, P. Magni, Bottom-up engineering of biological systems through standard bricks: a modularity study on basic parts and devices. *PLoS ONE* **7**, e39407 (2012). doi:10.1371/journal.pone.0039407 Medline

26. P. Siuti, J. Yazbek, T. K. Lu, Synthetic circuits integrating logic and memory in living cells. *Nat. Biotechnol.* (2013). doi:10.1038/nbt.2510 Medline

27. L. Qi, R. E. Haurwitz, W. Shao, J. A. Doudna, A. P. Arkin, RNA processing enables predictable programming of gene expression. *Nat. Biotechnol.* **30**, 1002 (2012). doi:10.1038/nbt.2355 Medline

28. G. F. Hatfull *et al*., Complete genome sequences of 138 mycobacteriophages. *J. Virol.* **86**, 2382 (2012). doi:10.1128/JVI.06870-11 Medline

29. https://biobricks.org/bpa/

30. N. L. Lee, W. O. Gielow, R. G. Wallace, Mechanism of araC autoregulation and the domains of two overlapping promoters, Pc and PBAD, in the L-arabinose regulatory region of Escherichia coli. *Proc. Natl. Acad. Sci. U.S.A.* **78**, 752 (1981). doi:10.1073/pnas.78.2.752 Medline

31. J.-D. Pédelacq, S. Cabantous, T. Tran, T. C. Terwilliger, G. S. Waldo, Engineering and characterization of a superfolder green fluorescent protein. *Nat. Biotechnol.* **24**, 79 (2006). doi:10.1038/nbt1172 Medline

32. R. Lutz, H. Bujard, Independent and tight regulation of transcriptional units in Escherichia coli via the LacR/O, the TetR/O and AraC/I1-I2 regulatory elements. *Nucleic Acids Res.* **25**, 1203 (1997). doi:10.1093/nar/25.6.1203 Medline

33. R. P. Shetty, D. Endy, T. F. Knight, Jr., Engineering BioBrick vectors from BioBrick parts. *J Biol Eng* **2**, 5 (2008). doi:10.1186/1754-1611-2-5 Medline

34. R. F. Wang, S. R. Kushner, Construction of versatile low-copy-number vectors for cloning, sequencing and gene expression in Escherichia coli. *Gene* **100**, 195 (1991). doi:10.1016/0378-1119(91)90366-J Medline

35. A. Haldimann, B. L. Wanner, Conditional-replication, integration, excision, and retrieval plasmid-host systems for gene structure-function studies of bacteria. *J. Bacteriol.* **183**, 6384 (2001). doi:10.1128/JB.183.21.6384-6393.2001 Medline

36. D. G. Gibson *et al*., Enzymatic assembly of DNA molecules up to several hundred kilobases. *Nat. Methods* **6**, 343 (2009). doi:10.1038/nmeth.1318 Medline

37. J. C. Anderson, C. A. Voigt, A. P. Arkin, Environmental signal integration by a modular AND gate. *Mol. Syst. Biol.* **3**, 133 (2007). doi:10.1038/msb4100173 Medline

38. K. Rinaudo *et al*., A universal RNAi-based logic evaluator that operates in mammalian cells. *Nat. Biotechnol.* **25**, 795 (2007). doi:10.1038/nbt1307 Medline

39. M. N. Win, C. D. Smolke, Higher-order cellular information processing with synthetic RNA devices. *Science* **322**, 456 (2008). doi:10.1126/science.1160311 Medline

40. J. E. Bronson, W. W. Mazur, V. W. Cornish, Transcription factor logic using chemical complementation. *Mol. Biosyst.* **4**, 56 (2008). doi:10.1039/b713852k Medline

41. B. Wang, R. I. Kitney, N. Joly, M. Buck, Engineering modular and orthogonal genetic logic gates for robust digital-like synthetic biology. *Nat. Commun.* **2**, 508 (2011). doi:10.1038/ncomms1516 Medline

42. T. Miyamoto *et al*., Rapid and orthogonal logic gating with a gibberellin-induced dimerization system. *Nat. Chem. Biol.* **8**, 465 (2012). doi:10.1038/nchembio.922 Medline

43. J. J. Lohmueller, T. Z. Armel, P. A. Silver, A tunable zinc finger-based framework for Boolean logic computation in mammalian cells. *Nucleic Acids Res.* **40**, 5180 (2012). doi:10.1093/nar/gks142 Medline

44. V. K. Mutalik *et al*., Precise and reliable gene expression via standard transcription and translation initiation elements. *Nat. Methods* **10**, (2013). 10.1038/nmeth.2404 Medline